

**BURIED PIPE LIFE PREDICTION IN SEWAGE TYPE
ENVIRONMENTS**

by

Jean-Matthieu Bodin

Thesis submitted to the Faculty of the
Virginia Polytechnic Institute and State University
in partial fulfillment of the requirements for the degree of

MASTER OF SCIENCE

in

Engineering Mechanics

Scott W. Case, Chair
Kenneth L. Reifsnider
Michael W. Hyer

August, 1998
Blacksburg, Virginia

Keywords: Life Prediction, Damage Accumulation, Buried Pipe

Copyright 1998. Jean-Matthieu Bodin

BURIED PIPE LIFE PREDICTION IN SEWAGE TYPE ENVIRONMENTS

by

Jean-Matthieu Bodin

Scott W. Case, Chair

Engineering Science and Mechanics

(ABSTRACT)

In this study, we develop a method of life prediction of buried pipe using the concepts of a characteristic damage state and damage accumulation. A stress analysis corresponding to the different types of load during service with environmental effects, a moisture diffusion model, and a lifetime prediction analysis combining the above models has been constructed. The model uses an elasticity solution for axial-symmetric loading in the case of pressurized pipe, and an approximate non-linear solution for transverse loading due to soil pressure in the case of buried pipe. The axial-symmetric stress analysis has been constructed taking into account the moisture content and the temperature of each ply of the laminate. The moisture diffusion model takes into account the geometry of the laminate, the different diffusivity coefficients in each ply, and also the geometric changes due to ply failure. The failure mode and material behavior of the pipe has been investigated and identified according to Owens Corning data. Thus, the code that has been developed allows one to predict the time to failure of Owens Corning industrial pipes under any time-dependent profile of environmental and loading conditions.

DEDICATION

A Kristin

This work is dedicated to my goldfish, Tic and Tac, and Indiana, my crayfish.

ACKNOWLEDGEMENTS

The author would like to thank the following people:

Dr. Scott Case who put up with me all year. This research wouldn't have been possible without his help, ideas, and advice.

Dr. K. L. Reifsnider for offering the author a position as research assistant in the Materials Response Group.

Dr. M. W. Hyer for his help, advice, and understanding.

Tozer Bandorawalla and Jeremy Duthoit for their enormous help on this project. I would especially like to thank them for their help with the moisture diffusion model, Mathematica, and their work on the mechanics of composite strength and life project.

Celine Mahieux, Sneha Patel, Byung Ki Ahn, Xinyu Huang, Fred MacBagonluri, Mike Pastor, Rob Carter, and all the members of the MRG for their support, their help, their advice, and for making me feel closer to home this year.

A special thanks to Blair Russell whose experience and advice helped me survive this year. He is a good friend, a very cool diving buddy, and an excellent adviser in the matter of choosing a driver.

Kristin, for her help and her moral support.

The members of my family, who have always been with me.

Madame Robinneau, for having been the principal instigator in my exclusion from high school and without whom I would probably never have arrived here.

Owens Corning for its financial support.

TABLE OF CONTENTS

I INTRODUCTION AND LITERATURE REVIEW.....	1
I.1 Introduction.....	1
I.2 Literature Review	2
I.2.a <i>Stress Analysis of Composite Pipe</i>	2
I.2.a.i Axial-Symmetric Stress Analysis.....	3
I.2.a.ii Bending Loads.....	8
I.2.b <i>Environment Constraints in Industrial Pipe</i>	14
I.2.b.i Soil Environment and Pipe Material.....	14
I.2.b.ii Polyester Aging and Moisture Absorption.....	17
I.2.b.iii Material Failure Function and Remaining Time to Rupture.....	18
II EXPERIMENTAL CHARACTERIZATION.....	21
II.1 Mechanical Phenomena in the Owens Corning Pipe.....	21
II.1.a <i>Owens Corning Pipe</i>	21
II.1.a.i Geometry.....	21
II.1.a.ii Materials Properties	24
II.1.b <i>Failure Mode of Owens Corning Pipe in Service</i>	27
II.1.b.i Pressure Test (Hydrostatic Design Basis HDB)	27
II.1.b.ii Ring Bending Test.....	28
II.2 Environmental Effects	29
II.2.a <i>Modulus, Strength, and Coefficient of Thermal Expansion (CTE) Changes with Temperature</i>	29
II.2.b <i>Modulus and Strength Losses with Water Content</i>.....	32
II.3 The Weeping Phenomenon.....	32
II.3.a <i>Mechanical Point of View</i>	32
III ANALYSIS AND MODELS.....	34
III.1 Analysis	34
III.1.a <i>Stress Analysis</i>	34
III.1.b <i>Moisture Absorption Analysis</i>.....	47
III.1.c <i>Life Prediction Analysis</i>	48
III.1.c.i Failure Function and Remaining Time to Rupture	48
III.1.c.ii Life Prediction Method.....	49
III.2 Models	51
III.2.a <i>Stress Analysis</i>	51
III.2.a.i Bending Model	51
III.2.a.ii Superposition of Bending and Pressure Model	61

III.2.b <i>Moisture Absorption Model</i>	62
III.2.c <i>Life Prediction Model</i>	63
IV RESULTS AND CONCLUSIONS	68
IV.1 Results of Calculations	68
IV.1.a <i>Results for Burst Pressure Life Prediction</i>	68
IV.1.b <i>Results for Ring Bending Life Prediction</i>	75
IV.2 Conclusions and Directions for Future Research.....	81
REFERENCES	85
APPENDIX: MATHEMATICA CODE	89
VITA	112

LIST OF ILLUSTRATIONS

Figure 1: Different Loading Conditions for Pipes	2
Figure 2: Coordinate System and Nomenclature, Hyer and Rousseau [4].....	4
Figure 3: Hydrostatic Strain Corrosion Test, McGrath <i>et al.</i> [11].....	13
Figure 4: Model of Fracture Processes Occurring in Aligned GRP Structures Tested in Air, Hogg and Hull [12]:	15
Figure 5: Model of Fracture Processes in Aligned GRP Structures Tested in Corrosive Environment, Hogg and Hull [12]:.....	16
Figure 6: Pipe Geometry	23
Figure 7: Tensile Test of Dried Sample in the Axial Direction of the Pipe	25
Figure 8: Tensile Test of Water Saturated Sample in the Axial Direction of the Pipe	26
Figure 9: Illustration of Elliptic Shape of Aluminum Pipes in Compression	35
Figure 10: Illustration of Elliptic Shape of PVC Pipes in Compression.....	36
Figure 11: Schematic of Ring Bending Test illustrating Strain Gage Locations	37
Figure 12: Experimental and Predicted Deflection versus Load for PVC Pipe	38
Figure 13: Experimental and Predicted Deflection versus Load for Aluminum.....	39
Figure 14: Experimental Strain versus Load for Aluminum.....	40
Figure 15: Experimental and Predicted Bending Strain/Load for Aluminum	41
Figure 16: Coordinate System for ANSYS Analysis	42
Figure 17: Deformed Shape and Meshing with Finite Element Analysis (Aluminum)...	43
Figure 18: Normalized Radial Displacement from ANSYS Analysis	44
Figure 19: Normalized Tangential Displacement from ANSYS Analysis.....	45
Figure 20: Diagram of the Life Prediction Code.....	49
Figure 21: Model for Castigliano’s Second Theorem	53
Figure 22: Burst Pressure Test at Room Temperature for 600 mm Diameter Flowrite Pressure Pipe: Data, Prediction.....	69
Figure 23: F_a and F_r Functions versus Time for an Initial Hoop Strain of 1.172% (45 bar).....	71
Figure 24: F_a and F_r Functions versus Time for an Initial Hoop Strain of 0.991%.....	72

Figure 25: F_a and F_r Functions versus Time for an Initial Hoop Strain of 0.925%..... 73

Figure 26: F_a and F_r Functions versus Time for an Initial Hoop Strain of 0.682%..... 74

Figure 27: Ring Bending Test at Room Temperature for 600 mm Diameter Flowrite in
Acid Environment: Data, Prediction..... 76

LIST OF TABLES

Table 1: Shape Factor in Equation 1.2.11 versus Pipe Stiffness.....	11
Table 2: Owens Corning Flowrite Pipe Laminate Geometry and Composition	22
Table 3: Mechanical Properties for Each Ply of the Laminate.....	24
Table 4: Coefficients of the Polynomial Equation of Matrix Properties Change with Temperature.....	30
Table 5: Environmental Effect Coefficient for Pipe Materials at 23° C	31
Table 6: Theoretical and Experimental Results for a 100 N Load.....	46

I INTRODUCTION AND LITERATURE REVIEW

I.1 Introduction

The goal of the present study is to construct a methodology that is capable of predicting the lifetime of Glass Fiber Reinforced (GFR) Polyester pipe in terms of the properties and performance of the constituents, the geometry and arrangements of those constituents, and the nature of the interface/interphase regions.

The pipe to be studied was designed by Owens Corning and is used as sewage pipe, buried pipe, and pressure pipe. These pipes must withstand pressure load, soil pressure, and accidental impact during installation. Impact damage refers to delamination of the composite at a discrete location. It creates a weak area where cracks can originate during service and cause unpredicted early failure.

In addition, the pipes are exposed to an aggressive environment which includes sewage, differing temperatures, and water of varying acidity. Water absorption is here a major factor in the lifetime of the pipe because it changes the stress analysis with time and its leakage may determine the effective end of service of the pipe. The environmental effects on the properties and the performance of the constituents also play an important role in the lifetime of the pipe.

1.2 Literature Review

1.2.a *Stress Analysis of Composite Pipe*

The analysis of composite pipes has been developed extensively in the various sectors of the pipe industry, including the oil industry (see Frost and Cervenka [1]) and the buried pipe industry (see Buczala and Cassidy [2]). These pipes are usually subjected to loading conditions of five types: pressure, transverse force, axial torque, axial force, and bending moment. This study focuses on the first two load types (Figure 1) because internal pressure and soil pressure, which can be reduced to a transverse load, are the major loads in the damaging process during service of buried composite pipe.

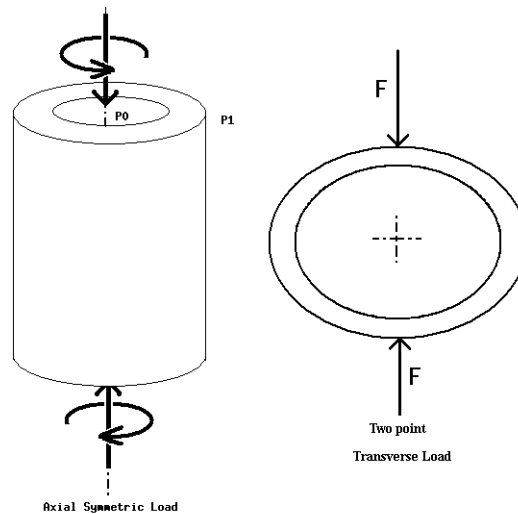


Figure 1: Different Loading Conditions for Pipes

I.2.a.i Axial-Symmetric Stress Analysis

Luo and Sun [3] develop an elasticity solution for stress-strain analysis in a bi-axial loading condition. They demonstrate a method for calculating the stress and strain of the pipes. Their analysis is applicable only to the case of axially symmetric loading with or without end effects. Thus, this analysis may be applied to the conditions of internal pressure, external pressure, axial load, and axial torsion. This solution assumes that there is no shear stress on the edge, that the normal stresses are continuous through the different layers, and that the cylinder is infinitely long.

Hyer and Rousseau [4] use the same assumptions to develop their thermo-elastic stress-strain analysis. The strain-displacement relations, the constitutive equations, the equilibrium equations and the strain compatibility equations are applied to each layer. The environmental factors of temperature and moisture are considered to be spatially uniform and independent of the coordinates θ and x (Figure 2). The axial symmetry of the geometry and loads allows them to disregard every derivative in θ or x in the differential equations of equilibrium. The environmental effect of moisture is not included in this study; however, because swelling stresses behave in the same way as thermo-elastic stress, it is easy to integrate moisture into this solution.

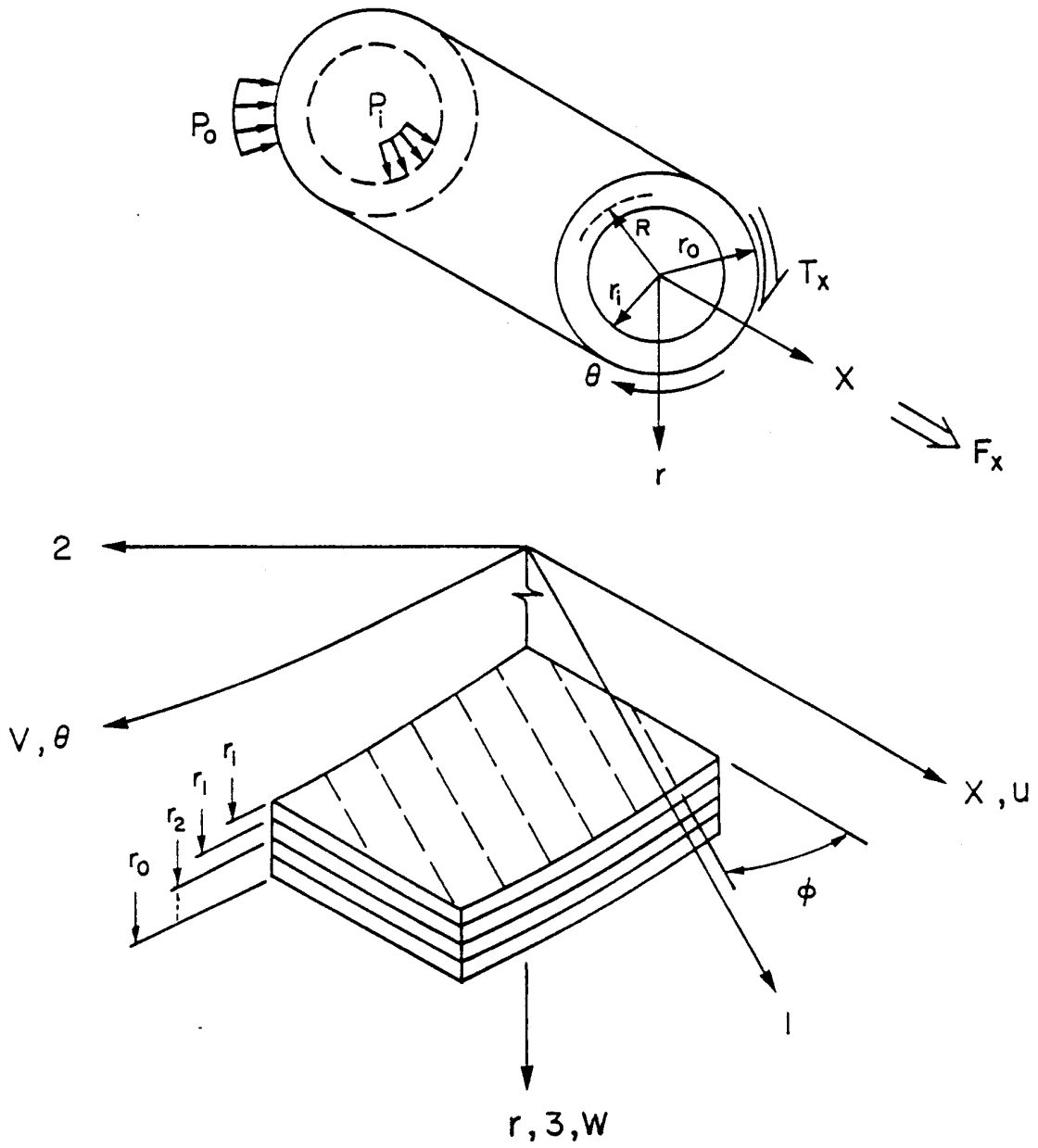


Figure 2: Coordinate System and Nomenclature, Hyer and Rousseau [4]

Hyer and Rousseau assume that the normal strain in the x direction, ε_x , and the shear strain $\gamma_{x\theta}$ are constant and equal to ε_0 and γ_0 for each layer because this is the case in an infinitely long cylinder. The resulting simplifications of the differential equation allow Hyer and Rousseau to create a general solution for the radial displacement, $W(r)$ (Figure 2 above). This general solution has four unknowns for each ply, but as previously stated, ε_0 and γ_0 are the same for each ply. The general solution for $W(r)$ is the following:

$$W(r) = A_i r^{\lambda_i} + B_i r^{-\lambda_i} + \left(\frac{C_{12}^i - C_{13}^i}{C_{33}^i - C_{22}^i} \right) \varepsilon_0 r + \left(\frac{C_{26}^i - C_{36}^i}{4 C_{33}^i - C_{22}^i} \right) \gamma_0 r^2 + \left(\frac{\Sigma^i}{C_{33}^i - C_{22}^i} \right) r \quad (1.2.1)$$

Where

$$\Sigma^i = (C_{13}^i - C_{12}^i) \varepsilon_x^T + (C_{23}^i - C_{22}^i) \varepsilon_\theta^T + (C_{33}^i - C_{23}^i) \varepsilon_r^T + (C_{36}^i - C_{26}^i) \gamma_{x\theta}^T \quad (1.2.2)$$

And

$$\lambda_i = \sqrt{\frac{C_{22}^i}{C_{33}^i}} \quad (1.2.3)$$

The constants C_{jk}^i are the j^{th} , k^{th} element of the stiffness matrix in the laminate coordinates of the i^{th} ply. The constants A_i and B_i are different for each layer and must be determined. The strains are obtained with the strain-displacement relations simplified for this axial-symmetric case:

$$\varepsilon_x = \varepsilon_0 \quad (1.2.4)$$

$$\varepsilon_\theta = \frac{W}{r} \quad (1.2.5)$$

$$\varepsilon_r = \frac{dW}{dr} \quad (1.2.6)$$

$$\gamma_{r\theta} = 0 \quad (1.2.7)$$

$$\gamma_{xr} = 0 \quad (1.2.8)$$

$$\gamma_{\alpha x} = \gamma_0 \quad (1.2.9)$$

The stresses are obtained from the strains with the constitutive equations.

For an N -layer laminate composite pipe, there are four major **boundary conditions**:

- The applied axial load is equal to the resultant of the axial stresses (one equation).
- The applied torque is equal to the resultant of tangential shear stresses (one equation).
- The radial stress on the inside of the first layer is equal to the internal pressure (one equation).
- The radial stress on the outside of the last layer is equal to the external pressure (one equation).

For an N -layer laminate composite pipe, there are two major **continuity conditions**:

- The stress continuity requirements between two adjacent layers give $N-1$ equations. The radial stress $\sigma_{rr}(r)$ at the interface between two adjacent layers is the same.
- The displacement continuity requirements between two adjacent layers also give $N-1$ equations. The radial displacement $W(r)$ between two adjacent layers is the same.

The displacement equations have $2*N+2$ unknowns. Therefore, the resulting stress analysis requires the solution of $2*N+2$ equations. The analysis includes the stresses developed by differences in thermal expansion and moisture swelling coefficients (Equation 1.2.2 on p. 5). They are integrated as constant values in the displacement equations. The code developed in this study for the lifetime prediction is based on this work.

I.2.a.ii **Bending Loads**

In most cases of buried pipe, the load during service is due to the soil pressure on the external side, which means that the main force in the static loading of non-pressurized buried pipe is the transverse load.

According to the American Water Works Association (AWWA) Manual [5], the vertical soil load on the pipe may be considered to be the weight of the rectangular prism of soil directly above the pipe. The soil prism has a height equal to the depth of earth cover and a width equal to the outside diameter of the pipe.

$$W_c = \frac{\gamma_s H}{144} \tag{1.2.10}$$

Where W_c is the vertical soil load in psi, γ_s is the unit weight of overburden in lb/ft³; that is, weight per unit volume of soil, and H is the burial depth of the top of the pipe in feet.

The literature provides considerable information on the problems of laminated composite pipe. Although it also deals with buried laminated composite pipe (see Buczala and Cassady [2]), an exact stress analysis does not exist for the case of pure transverse load.

Pagano [6] develops an elasticity solution for the displacement of an infinitely long tube under an applied axial bending moment; however, the analysis is limited to the case of a single layer of material.

Fuchs and Hyer [7] present a means to analyze the bending response of thin-walled laminated composite cylinders. Their analysis employs Donnell's shell theory for the kinematics. However, unlike in Pagano's analysis [6], multiple material layers may be analyzed. In addition, the analysis may be used to investigate the behavior of finite-length cylinders. By integrating the equilibrium equations, it is possible to calculate the inter-laminar stresses. This solution has been developed for a bending moment due to forced edge displacement.

Claydon *et al.* [8] develop a model for the analytical determination of pipe stiffness, interlayer contact pressure, stress recovery, slippage between layers, wear, and fatigue for a helical wound flexible pipe. The model presented in their paper is based on the assumptions of small displacements and small strains, as well as constant axial and pressure loads (the bending stress is superposed). Additionally, a thin-walled theory is applied to each of the layers. The helix is constrained from rotation and the radial displacement is constant through the thickness (a direct result of the thin-wall assumption). Finally, laminate thickness is ignored in the development of the radial equilibrium relations, so that the total pressure differential is equal to the sum of the individual layer pressure differentials.

Pearson [9] provides a testing methodology for fiberglass pipe products in bending for the AWWA. The Hydrostatic Design Basis (HDB) test, ASTM D2837, was created to predict the serviceability of the pipe during long-term (over 50 years) loading. The pipe is placed between two plates and the deflection is set. The pipe fails when the liquid leaks to the outer skin (“weeping failure”) and/or when a burst occurs. The strain is computed with the following experimental formula:

$$\varepsilon_b = Df \frac{t \delta}{D^2} \tag{1.2.11}$$

Where t is the pipe thickness, δ is the deflection, D is the pipe diameter, and Df is a shape factor experimentally evaluated according to the pipe stiffness (PS) (Table 1):

Table 1: Shape Factor in Equation 1.2.11 versus Pipe Stiffness

PS in kPa	Df non Dim.
62	8
124	6.5
248	5.5
496	4.5

A minimum strain is defined by extrapolating tests conducted on one class of pipes over 50 years. The tests were conducted following the guidelines of ASTM standard “Long-Term Ring Bending of Fiber Glass Pipe” D2837. This procedure involves monitoring the time to failure under constant load of a series of pipe ring samples. The long-term ring bending strain is obtained by extrapolation to fifty years of a log-log linear regression line for failure strain (deflection) versus time. All tests were conducted with the pipe rings totally immersed in the test fluid. Nominal temperature was 23° C. Load was applied to the pipe ring by flat plates at the top and bottom. For each sample the increase in deflection versus time was recorded. Failure was taken as either rupture of the pipe wall or the point at which the sustained slope of the log-deflection (or log strain) versus log time line between subsequent readings reaches 0.25 or greater.

The ASTM D3681 standard gives the failure strains established from the failure deflection by:

$$\varepsilon = \frac{4.88 t \delta}{\left(D + \frac{\delta}{2}\right)^2} \quad (1.2.12)$$

This formula is an approximation of the theory of isotropic materials that is presented in Chapter III.2.a.i, Equation 3.2.23.

The extrapolation over fifty years of a log-log linear regression line for failure strain (deflection) versus time may overestimate the actual long-term strength, according to Mruk [10] in his study on long-term HDB tests. The data presented by Mruk in a log-log plot appear linear until 10,000 hours of service; nevertheless, in some cases, a downturn of the strength may occur and failure could arise after considerably less time than projected.

McGrath *et al.* [11] use a fixture as shown in Figure 3 to evaluate the evolution of the modulus of the pipe during service load profile. They apply a deflection to the pipe that produces a specific strain. The load is taken to be equivalent to the long-term load due to the soil compression. They also superimpose, at a given time interval, an extra load corresponding to short-term load such as automobile traffic. The results show a relaxation of the long-term bending modulus of the pipe. The slope dF/dy (load over

deflection) decreases with time. Despite this phenomenon, superimposed short-term load tests performed during the long-term load test show the same modulus at all times. This was true even when the prior deflection levels had exceeded the linear visco-elastic limits.

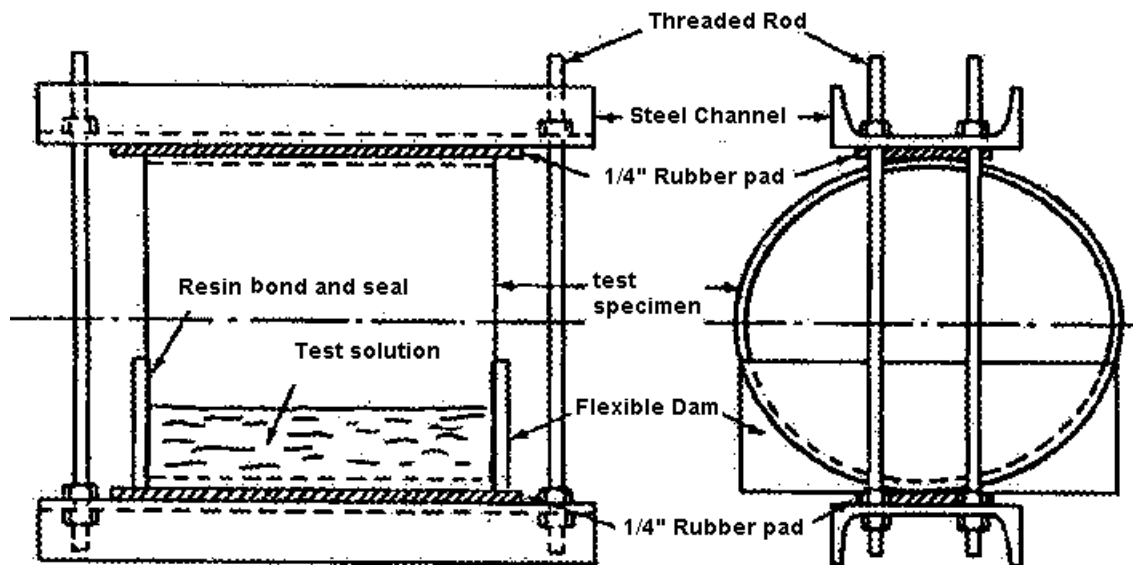


Figure 3: Hydrostatic Strain Corrosion Test, McGrath *et al.* [11]

Ring bending tests performed by Hogg and Hull [12] on E-glass fiber reinforced polyester composite pipe (76 mm in diameter and 1.8 mm in thickness) in an air environment and a corrosive environment show linear load versus deflection behavior, and linear load versus strain behavior (1.5% tensile strain and 25% deflection); this may seem to justify using a linear theory. In Chapter III.2.a.i, however, we show that in fact a non-linear theory is preferable for our purposes. The deformed shape is initially an

ellipse, which becomes flattened at the face of the compression plates (top and bottom) as load is applied.

I.2.b Environment Constraints in Industrial Pipe

In order to more accurately model the real conditions of pipe service, we define a list of environmental factors to be considered in building an understanding of the effects of these factors on the damage processes and the pipe lifetime. The studied pipe is used for sewer and wastewater. The pipes are buried, so they are under soil environmental effects such as moisture, corrosive liquid, local corrosion and impact effects during installation.

I.2.b.i Soil Environment and Pipe Material

Hogg and Hull [12] study the nucleation and propagation of cracks in aligned continuous glass fiber reinforced polyester composites in the presence of hydrochloric acid (H-Cl). The tests were performed using the ring bending test standard ASTM 2837 (parallel plate compression). Two types of cracks were created during the test due to strain deformation and corrosion: planar cracks, which are normal to the fiber direction, and inter-laminar cracks between planar cracks. The authors report important relations between environment and stresses in the influence of environmental effects. The type of fracture also depends strongly on the acid type and concentration.

This last statement disagrees with Owens Corning data (see Pearson [13]). The study performed by Owens Corning shows very few changes between HDB stress bending (Sb) tests (pipe lifetime in ring bending test immersed in acid solution) at pH 4 and at pH 10. The result was no appreciable difference in the long-term ring bending strain for the two solutions. In fact, the test in water gave similar results to the test in different pH solutions.

According to Hogg and Hull [12] the propagation of cracks in air shows fiber debonding and matrix cracking as in Figure 4. In an acid environment, some fracture is initiated in individual fibers very close to the surface due to the acid attack as shown in Figure 5. The crack will produce a strain magnification in adjacent fibers and the penetration of acid will result in further cracking of fibers at the crack tip. The crack will propagate, facilitating acid propagation and weeping (as previously defined).

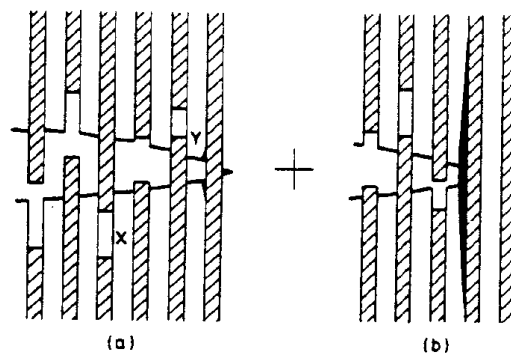


Figure 4: Model of Fracture Processes Occurring in Aligned GRP Structures Tested in Air, Hogg and Hull [12]:

a) fiber fracture and pull out; b) delamination

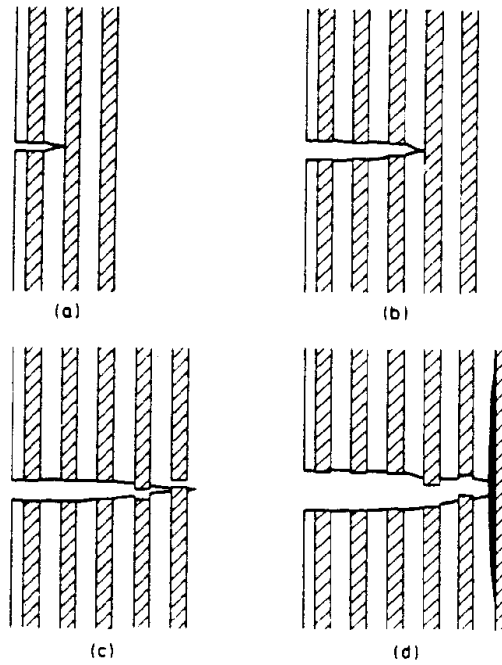


Figure 5: Model of Fracture Processes in Aligned GRP Structures Tested in Corrosive Environment, Hogg and Hull [12]:

a) nucleation of first crack by acid attack on fiber; b) growth of flat crack by fiber fracture at tip of resin crack; c) development of small amount of pull out due to out of plane fiber fracture; d) delamination cracks at tip of flat crack

I.2.b.ii Polyester Aging and Moisture Absorption

Loos *et al.* [14] compile a summary of the effects of moisture and temperature on the properties of chopped fiber reinforced sheet molding compounds. They observe the behavior of moisture absorption of glass fiber exposed to humid air or to liquid. Moisture absorption is defined as weight change with respect to time. This phenomenon depends on the material, the temperature, and the environment (relative humidity, type of liquid). The data show that the weight does not remain constant after reaching the saturation level. This may lead us to believe that the moisture transport is a non-Fickian process.

The differences with the Fickian model are admissible at room temperature, but increase with increased temperature. According to Loos *et al.* [14], cracks develop in the matrix due to swelling, stress, or temperature. As a result, the moisture content increases rapidly causing increase or decrease in weight by material loss (micro-particle loss due to cracks). However, according to the authors, under most conditions, Fick's law, together with values of the apparent diffusivity, may be used to approximate the weight change and the moisture content until the apparent maximum moisture content is reached.

This last assumption allows us to consider the case of moisture absorption applied to the Owens Corning pipe as a Fickian phenomenon. It also simplifies the lifetime prediction model.

Loos *et al.* [14] also report tensile strengths and modulus retained for several polyester-glass composite systems after exposure to different moisture environments for 30 and 180 days. After 180 days, all polyester-glass materials reach a minimum in their material properties. We use a curve-fit of these data for the properties versus moisture content in the life prediction code.

I.2.b.iii **Material Failure Function and Remaining Time to Rupture**

Frost and Cervenka [1] study the use of composite pipe in the oil industry. This field requires the material to have a minimum lifetime of twenty to thirty years. This study has helped develop an understanding of the failure mechanism and the different types and effects of environment and loading existing in this field of use, especially the roles of environment, temperature, and chemicals.

The pipes tested by Frost and Cervenka were composed of a $[\pm 55]_n$ Epoxy E-Glass reinforced filament-wound composite, 76 to 110 mm in diameter and approximately 5 mm thick, under an axial-symmetric pressure load. The pipes were filled with pressurized water or different types of chemical solutions such as alcohol, alkanes or aromatics. The pipe is considered failed when it starts to leak or weep. The weeping phenomenon occurs when drops of liquid appear on the surface of the pipe like tears. The long-term tests show a uniform leakage of the liquid over the entire external surface of the pipe after several thousand hours. A visual analysis of the damaged

composite proves that weeping results in through-thickness cracks within each ply, together with delamination, thereby forming a convoluted path through the pipe wall. In the case of filament wound GFR pipe, weeping appears after matrix failure in all plies, and fibers remain intact through the thickness. In the case of Owens Corning pipes the fibers are in the hoop direction. The stresses due to service load are also principally in the hoop direction. In this case, a maximum stress failure theory does not allow cracks in the matrix before cracks in the fiber. Following this statement, burst must occur before weeping. While this statement is true for the maximum stress failure criterion, we choose but it may not be true with other failure criteria.

Phillips [15] has conducted tests to determine the lifetime to failure versus stress for glass fiber reinforced composites in air. He also demonstrates statistically the reliability of his method. The tests were performed at different levels of stress and a relation based on Zhurkov's theory of fracture mechanics [16] was developed. One assumption of this theory is that the failure mode remains the same during the damaging process. The tests show that a relation between the ratio stress/strength and the delayed time to rupture can be constructed as follows:

$$\log(tr) = A - B \left(\frac{\sigma}{\sigma_o} \right) \text{ where } \frac{\sigma}{\sigma_o} = Fa \quad (1.2.13)$$

where A and B are constants that are highly dependant on the material and the environmental conditions, tr is the time to rupture, σ is the level of stress in the material, and σ_o is the ultimate strength (instantaneous rupture). The ratio of stress to ultimate strength stress is the failure function (denoted Fa). Thus, the time to rupture can be defined according to the failure function.

Hogg and Hull [12] affirm that failure is always associated with the region of tensile strain and not with the region of compression strain. Following this last statement, the logical way to allow weeping in ring bending is through cracks in the bottom where tensile strain is on the inside layer. Thus, there is propagation of the liquid through the pipe circumference via the inter-laminar crack (or the sand layer in the case of Owens Corning pipe), and finally cracks occur on the external layer of the side where there is tensile strain. This last hypothesis must be checked because it implies that failure criteria must be evaluated at two critical places: the side and the bottom. It also implies that the maximum stress failure criterion is a valid assumption for the life prediction under consideration.

II EXPERIMENTAL CHARACTERIZATION

II.1 Mechanical Phenomena in the Owens Corning Pipe

The present study is an attempt to build an understanding of life prediction of Owens Corning buried pipe for a sewage environment. The code developed is based on experiments conducted on this class of pipe. We begin with a description of the pipe and the existing data.

II.1.a *Owens Corning Pipe*

II.1.a.i Geometry

The tested pipes have a diameter of 600 mm; however, the model to be developed is applicable to every kind of geometry, as long as the ratio of radius over thickness is less than 10. This last stipulation is a result of the approximate transverse loading solution.

The test specimens were approximately two meters long. The pipes were produced from continuous hoop-wound glass fiber, chopped glass fiber, silica sand, and thermosetting polyester resin. The geometry and composition of the pipe wall are shown

in Table 2 and diagrammed in Figure 6, which outline the thickness of each ply and the material compositions.

Table 2: Owens Corning Flowrite Pipe Laminate Geometry and Composition

Ply	Thick. Mm	%Resin	%Hoop glass	%Glass Mat	%Chop. Glass	%Sand
Surf.Veil	0.20	90	0	10	0	0
Outer Skin	1.33	32	45	0	22	0
Core	4.74	27	2	8	0	63
Inner Skin	1.33	32	45	0	22	0
Liner	0.80	60	0	0	40	0
Surf.Veil	0.20	90	0	10	0	0

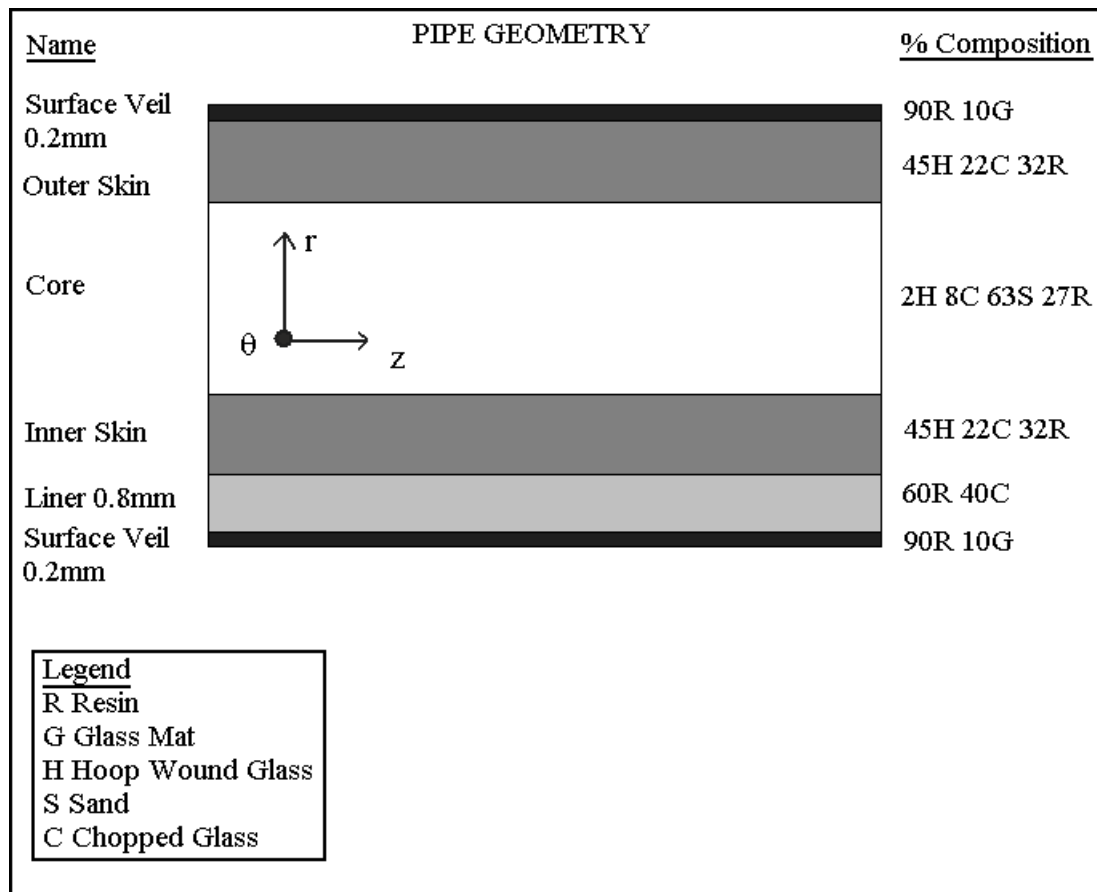


Figure 6: Pipe Geometry

II.1.a.ii Materials Properties

The properties of the plies at room temperature (23° C) and under dry conditions are reported in Table 3, based on data provided by Owens Corning:

Table 3: Mechanical Properties for Each Ply of the Laminate.

Properties	Surf.Veil	Liner	Inner Skin	Core	Outer Skin	Surf.Veil
E ₁ GPa	3.3	5.5	33	5	33	3.3
E ₂ GPa	3.3	5.5	12	4.8	12	3.3
E ₃ GPa	3.3	3.3	3.3	3.3	3.3	3.3
G ₁₂ GPa	1.32	2.1	3	2.1	3	1.32
ν_{12}	0.25	0.31	0.31	0.2	0.31	0.25
X _t MPa	74.9	133.1	590	58.9	590	74.9
Y _t MPa	65.9	96.5	60	22.7	60	65.9
X _c MPa	167	182.6	504.8	120	504.8	167
Y _c MPa	146.9	132	137	45	137	146.9

Tensile tests were performed on samples of a pipe section with a dimension of 25.4 x 127 mm. Because the width of the sample was small enough compared to the total diameter of the pipe, the sample was considered to be flat. The results of these tests on dried and water saturated samples (Figures 7 and 8, respectively) give the same results as tensile tests of the pipe in the axial direction; that is, a linear behavior of the stress-strain relation until 100000 N/m.

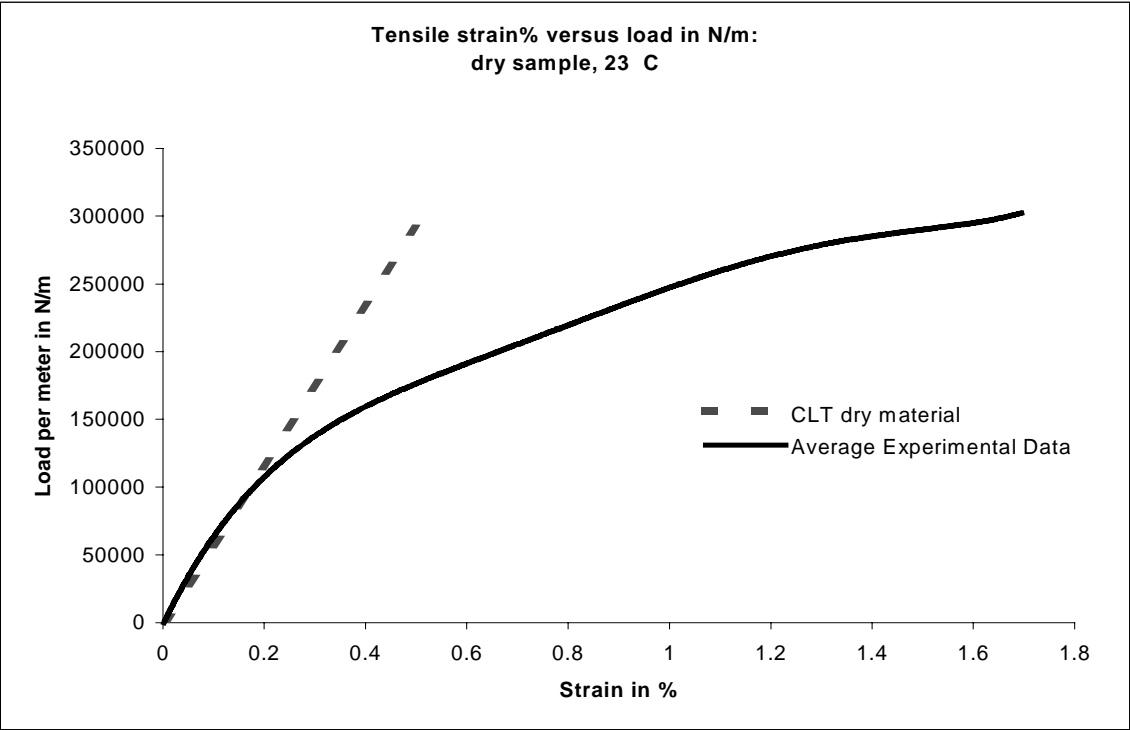


Figure 7: Tensile Test of Dried Sample in the Axial Direction of the Pipe

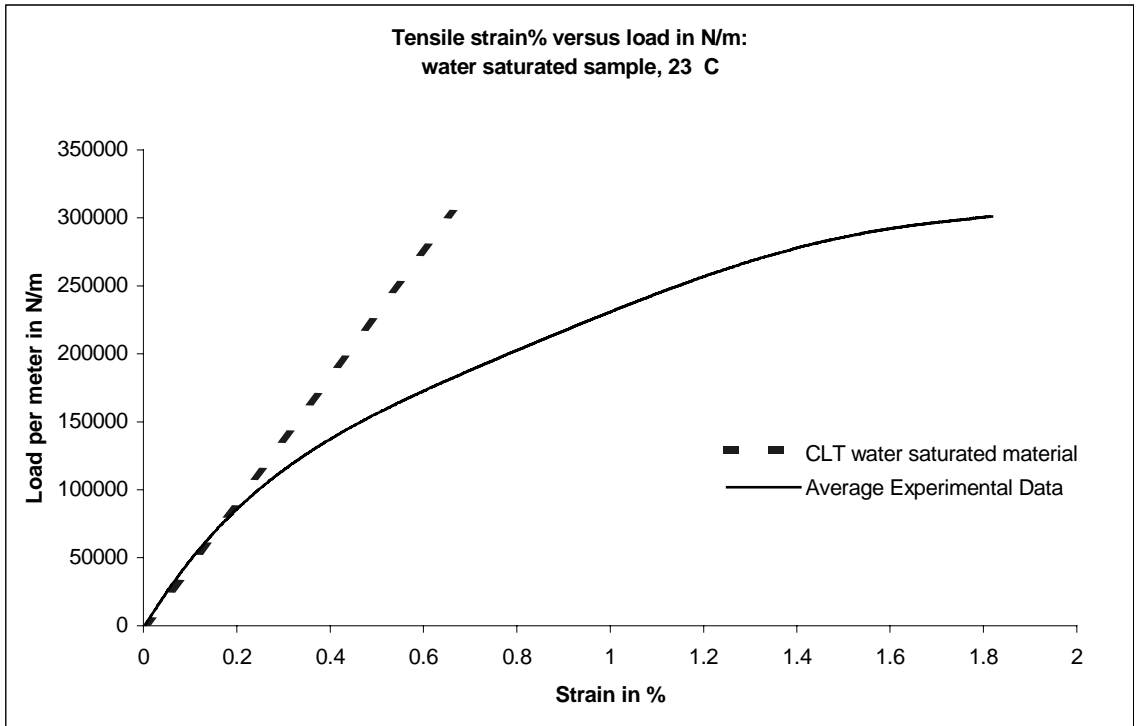


Figure 8: Tensile Test of Water Saturated Sample in the Axial Direction of the Pipe

Using the mechanical properties of the materials in Table 3 (p. 24), classical laminate theory gives a very close approximation of the experimental stress-strain relation. At a load greater than 100000 N/m, the slope of the load versus strain changes but the lamination theory does not indicate that the stresses are bigger than any strength value. The stress-strain behavior is still pseudo-linear with a different slope. And finally, the specimens break at a value close to the theoretical value computed with the maximum stress failure criterion.

The stress analysis shows that, in the case of a pressurized pipe and in the case of transverse load, the stresses in the axial direction are always smaller than the initial point of non-linearity shown in Figures 7 and 8 above. The material properties are thus validated, and we can say that no cracks exist due to these stresses, at least in the axial direction. We did not examine the properties in the hoop direction because only one pipe sample was provided for testing. The radius of the pipe provided was not large enough to cut flat samples in the hoop direction.

II.1.b Failure Mode of Owens Corning Pipe in Service

Several tests have been performed on Owens Corning pipe to estimate its lifetime under service loading conditions. The pressure test allows us to classify the pipe with maximum pressure evaluated with an extrapolation of the data over 50 years. The same method is used for the ring bending test; however, these data provide important information on the mode and reasons for failure of the pipe.

II.1.b.i Pressure Test (Hydrostatic Design Basis HDB)

The test procedure for the pressure test follows the guidelines of ASTM D2992-96 "Obtaining Hydrostatic or Pressure Design Basis for 'Fiber Glass' (Glass-Fiber-Reinforced Thermosetting-Resin) Pipe and Fittings -- Procedure B". According to Pearson [13] in his report for Owens Corning, the time to failure was determined as the passage of the test fluid (water) through the pipe wall. This was evidenced as "weeping",

which appears as moisture condensation on the outside of the pipe specimen. According to test reports, for cases in which there is weeping, the failure occurs first in the sand layers, then cracks appear in the internal hoop glass layers allowing pressure to enter, and finally the external hoop layer fails. The other case of failure is the situation in which burst occurs. The external layer strain, called “initial hoop strain” in Pearson’s report, is the recorded value versus time to rupture. The present study calculates the corresponding pressure of this strain, which is not mentioned in the report.

II.1.b.ii **Ring Bending Test**

As defined in Chapter I.2.a.ii, the failure in ring bending tests occurs either when there is rupture of the pipe wall or when the sustained slope of the log deflection versus log timeline between subsequent readings is 0.25 or greater. In tests performed on Flowrite Owens Corning pipe (600 mm in diameter), for all samples, the failure was by rupture of the wall. There is no mention in the Owens Corning report of how the rupture of the wall occurs. According to Hogg and Hull [12], the failure mode is total matrix failure, and the pipe leaks when cracks develop throughout the thickness.

Hogg and Hull’s statement, however, does not apply to the geometry of the Owens Corning pipe laminate, since it is composed with only pseudo-isotropic material such as chopped strand glass, sand-polyester, and anisotropic material oriented in the hoop direction as skin layers. There is no reason to expect delamination or matrix

cracking due to ply rotation as is observed to occur in the ring bending test for $[\pm 55]$ glass reinforced filament wound pipe. However, we assume here for the purposes of the ring bending tests, that matrix cracking can occur with the synergistic effects of transverse load and swelling stresses; this assumption is used to determine one of the failure functions in the code.

II.2 Environmental Effects

According to the tests done by Owens Corning and to Loos *et al.* [14] (see Chapter I.2.b.ii), the major environmental effects on the lifetime of the pipe are the temperature and the moisture content. Temperature and moisture content create thermal expansion and swelling stresses. The coefficients of thermal expansion can change with temperature. The environmental effects also change the properties of the material.

II.2.a Modulus, Strength, and Coefficient of Thermal Expansion (CTE)

Changes with Temperature

Owens Corning data [17] on the influence of temperature on materials gives the following polynomial equation for the modulus, the stiffness, and the CTE for the polyester matrix:

$$\text{Property}(T) = A + B T + C T^2 \quad (2.2.1)$$

where T is the temperature in Celsius and A , B , and C are reported in Table 4. The other materials are considered to have no property changes with temperature.

Table 4: Coefficients of the Polynomial Equation of Matrix Properties Change with Temperature

	A	B	C
Modulus MPa	3567	0.22	-0.15
Strength MPa	71.3	0.0062	-0.003
Thermal Expansion Coef. in °C ⁻¹	2.58e-5	9.31e-7	0

All the properties used in the code are evaluated at 23° C. The values used for lamina mechanical properties are the result of the rule of mixtures (ROM). The ROM is:

$$\text{Property}_{\text{composite}} = \sum (\% \text{ of } _ \text{Material} \times \text{Property}_{\text{Material}}) \quad (2.2.2)$$

The coefficients of swelling for the individual plies are determined by Agarwal and Broutman [18] based on swelling coefficients for unidirectional glass epoxy laminates, and are listed in Table 5.

Table 5: Environmental Effect Coefficient for Pipe Materials at 23° C

	Surf.Veil	Liner	Inner Skin	Core	Outer Skin	Surf.Veil
Thermal expansion Coef. α_1	4.2984e-5	3.0336e-05	1.84e-5	1.6423e-05	1.84e-5	4.2984e-5
Thermal expansion Coef. α_2	4.2984e-5	3.0336e-05	4.2984e-5	1.6423e-05	4.2984e-5	4.2984e-5
Swelling Coef. β_1 m/m.kg/kg	0.3	0.6	0	0.6	0	0.3
Swelling Coef. β_1 m/m.kg/kg	0.3	0.6	0.6	0.8	0.6	0.3
Saturation level kg/kg	0.036	0.295	0.035	0.04	0.035	0.036
Stiffness reduction %	10	20	20	40	20	10
Strength reduction %	35	20	11	40	11	35

The fiber direction of the hoop wound glass plies, inner and outer skins, are assumed to have no swelling strain, due to the effect of the continuous glass fibers. Also, slightly different swelling coefficients for each ply have been assumed based on the glass and silica sand content of each ply.

II.2.b *Modulus and Strength Losses with Water Content*

According to Springer [19], the material properties can be reduced using a linear function of the moisture content. The properties are reduced linearly according to the maximum moisture content, the maximum percentage of reduction, and the moisture content as shown in the following equation in which X_o is the initial value, and X is the reduced value:

$$X = X_o \left(1 - \frac{Max_reduction_ \% \times moisture_content}{moisture_content_{max}} \right) \quad (2.2.3)$$

We use Equation 2.2.3 to estimate the modulus and the strength according to the moisture content of the specimen. The values used in the code are those shown in Table 5 above.

II.3 **The Weeping Phenomenon**

II.3.a *Mechanical Point of View*

The different tests were performed by filling the pipe with water. For the hydrostatic tests, the weeping phenomenon was observed for certain pressures after a certain time. The model does not explain such effects because we expect the hoop fibers

in the pipe to crack before the matrix. The model predicts that the pipe should burst before leaking.

In the case of the ring bending test the weeping is due to cracks throughout the thickness, allowing liquid passage to the outside of the pipe. According to Owens Corning, the core fails first followed by the inner surface veil and the chopped material layer. Finally, the moisture enters into the thickness and the last two layers fail allowing the liquid to leak. The stresses are not uniformly distributed due to the geometry of the loading, so failure in the plies occurs very locally. Our assumption here is that the ply cracks locally and the liquid enters into the crack at this point. In all other areas of the pipe the stiffness of the layer remains the same. Although the stiffness of a failed ply is not uniform anymore, we discount the properties of the locally failed ply on the entire ply. Except at the location of the crack, where there is stress redistribution and moisture change, the pipe still maintains its form. Thus, there is the possibility that the pipe may leak without catastrophic failure.

III ANALYSIS AND MODELS

III.1 Analysis

III.1.a *Stress Analysis*

In order to validate the theoretical model, the assumptions upon which it is based must be verified. These assumptions are the following: the deformed shape remains elliptical at every load in the range of elastic strain; the stretching in the pipe can be disregarded with respect to the bending of the pipe; and the relations developed for an isotropic material can be applied to the Owens Corning composite pipe, if the appropriate bending stiffness terms are used.

To validate the above model assumptions, several compression tests were carried out with aluminum and PVC pieces of pipe. Figures 9 and 10 verify the first assumption (elliptical shape) for each material. In each of these Figures, an ellipse having the same width and height as the actual ring has been drawn. We notice that the ellipse represents well the shape of the ring. As a result, our model will be based on an elliptic deformed shape.

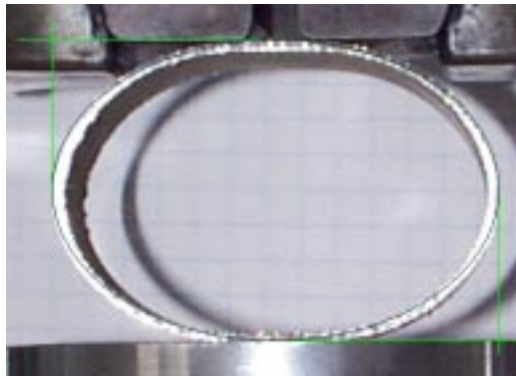
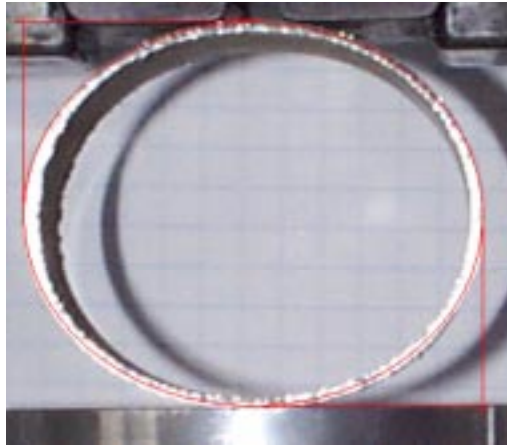
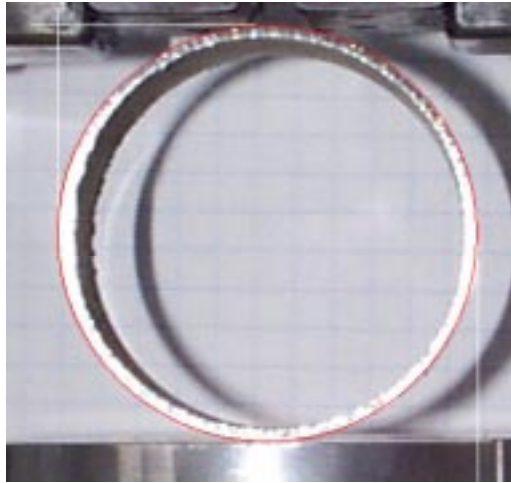


Figure 9: Illustration of Elliptic Shape of Aluminum Pipes in Compression

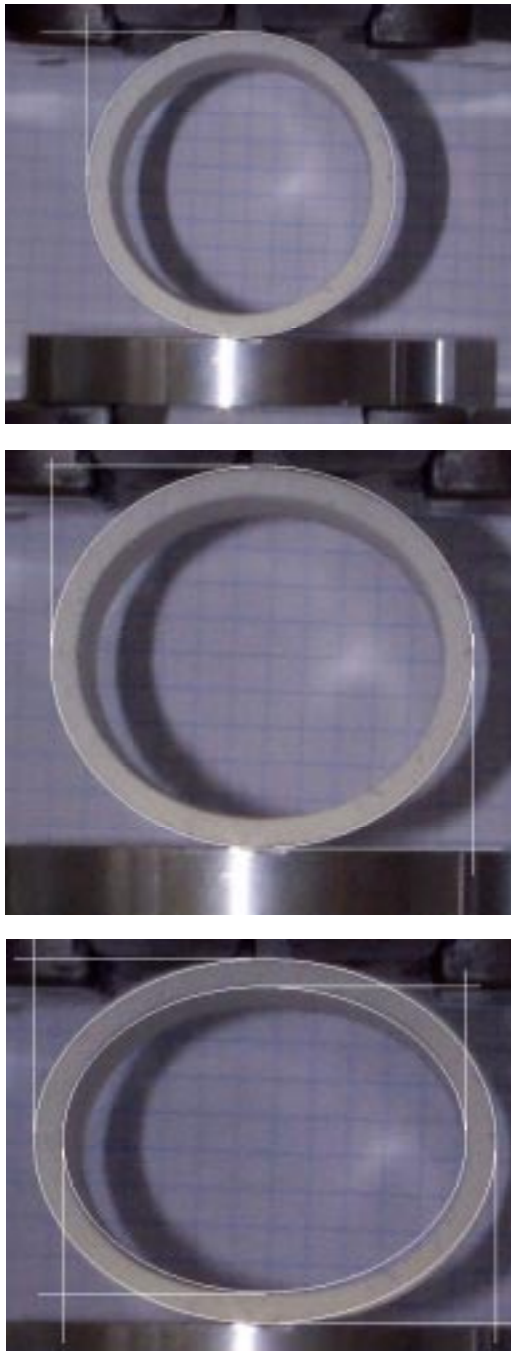


Figure 10: Illustration of Elliptic Shape of PVC Pipes in Compression

In order to further check the validity of the model, a compression test with strain gages was conducted. Strain gages were attached to both sides of an aluminum ring (point B in Figure 11, gages 1, 2, 3, 4), and the displacement, the strain and the load were recorded. These gages were placed on the inner and outer sides of the ring in order to ensure the validity of the measurement. The resulting data show that one gage (gage 3) was not well adhered but the other gage (gage 4) gives the same value as gage 2.

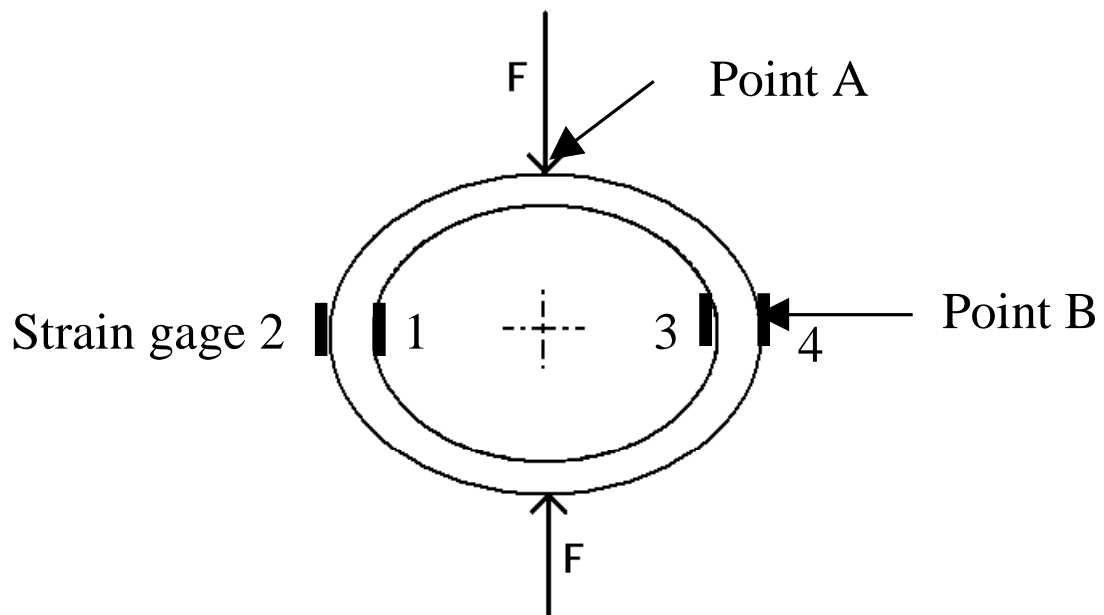


Figure 11: Schematic of Ring Bending Test illustrating Strain Gage Locations

With the experimental data of ring deflection versus applied load, we can evaluate the experimental pipe stiffness of the ring. The model computations (see Chapter III.2.a.i) are shown in the same chart as the experimental data for PVC pipe (Figure 12) and for aluminum pipe (Figure 13).

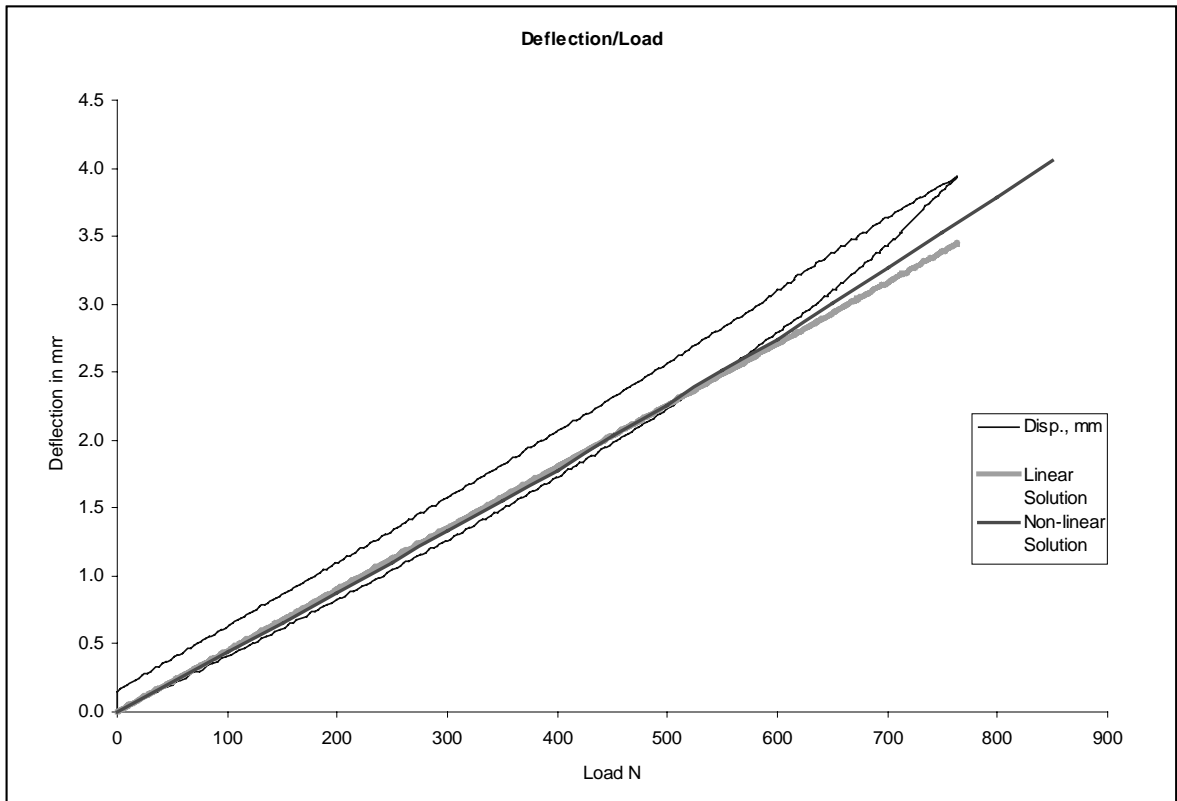


Figure 12: Experimental and Predicted Deflection versus Load for PVC Pipe

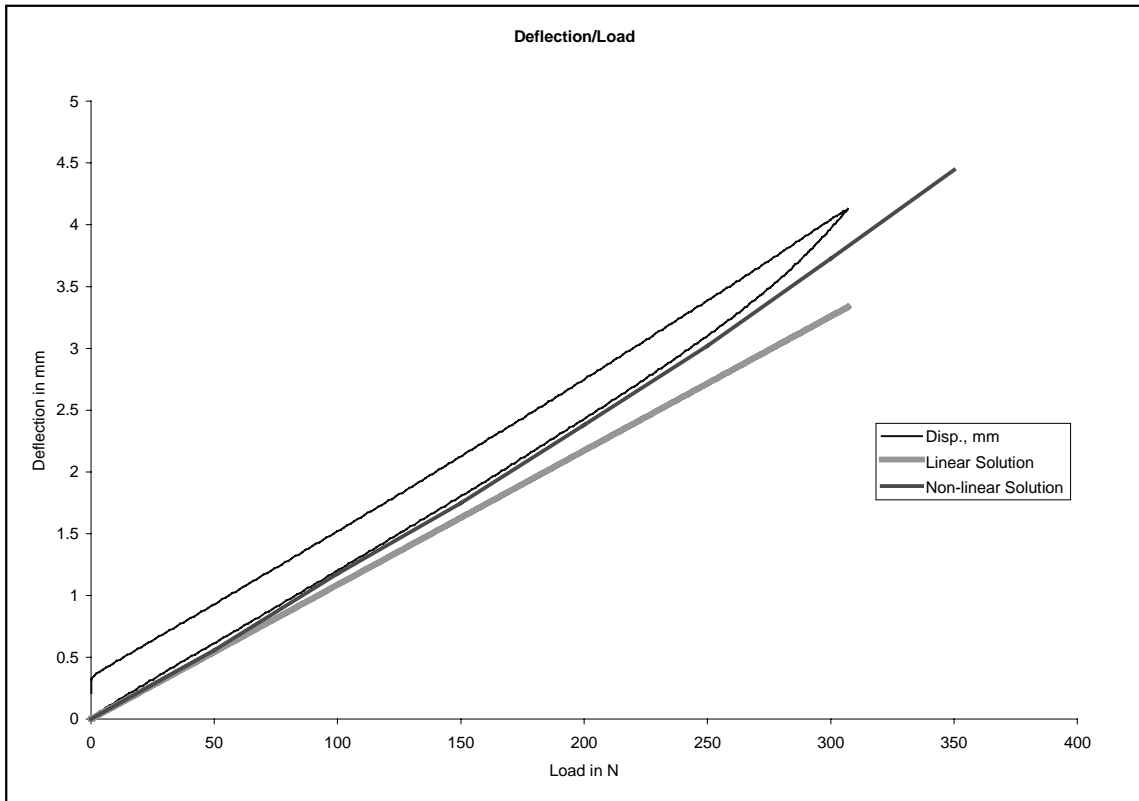


Figure 13: Experimental and Predicted Deflection versus Load for Aluminum

Using Equation 3.2.20 (p. 60) of the bending moment and the following equation we have the theoretical bending strain:

$$\epsilon_{\max} = \frac{M_b \times thickness}{2 E I} \quad (3.1.1)$$

where ϵ_{\max} is the maximum strain on the external side of the ring, M_b is the moment at this point, E is the tensile modulus, and I is the area moment of inertia of the ring section.

By subtracting the strain at gage 2 from strain at gage 1 (Figure 14) and dividing by 2 we obtain the pure experimental bending strain on the side of the ring. The comparison between the experimental strain and the predicted strain from the model we develop in Chapter III.2.a.i for aluminum is found in Figure 15. The results are almost identical, thereby validating the model.

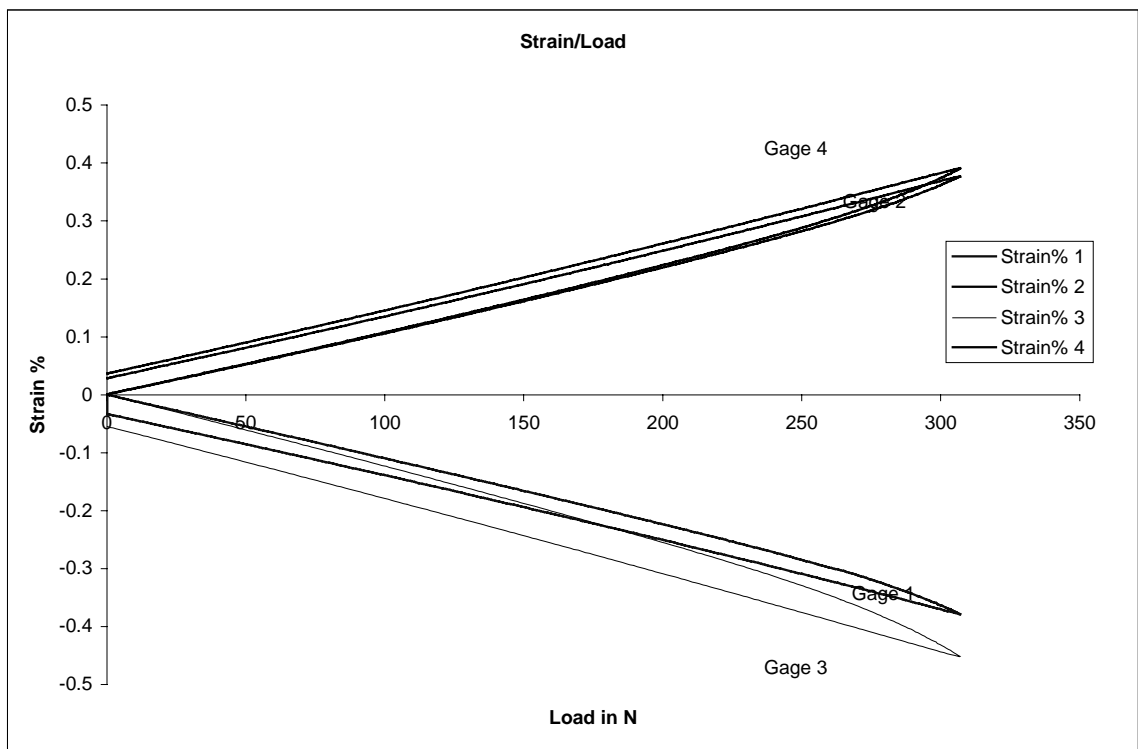


Figure 14: Experimental Strain versus Load for Aluminum

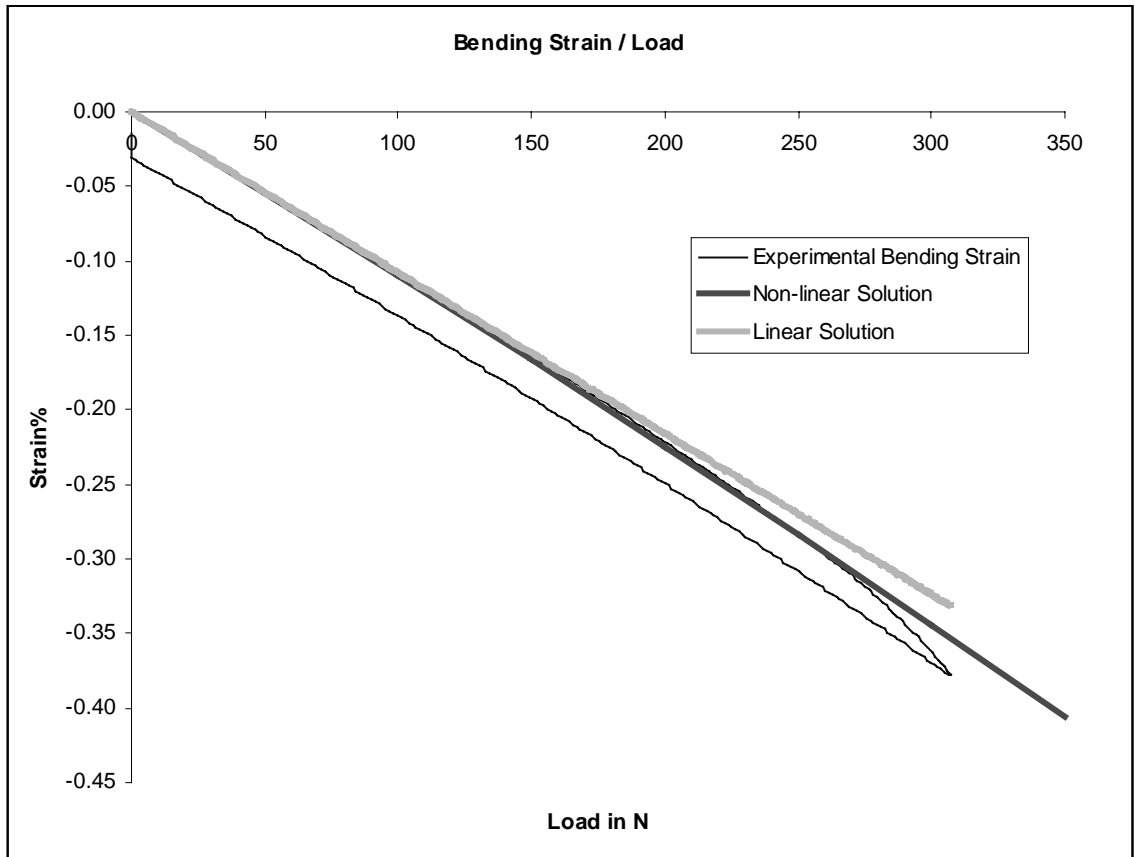


Figure 15: Experimental and Predicted Bending Strain/Load for Aluminum

Because the model used in the code takes into account the non-linearity of the large deformation, we examine the large deformation using the commercial finite element code, ANSYS, whose coordinate system is shown here in Figure 16:

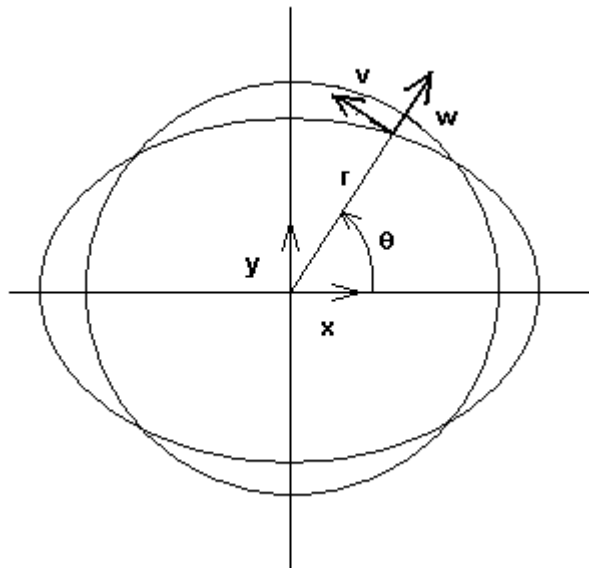


Figure 16: Coordinate System for ANSYS Analysis

Simulations of the compression test have been done with ANSYS at deflections corresponding to loads varying from 100 N to 1000 N with the same geometry as the aluminum ring tested in the present study (Figure 17).

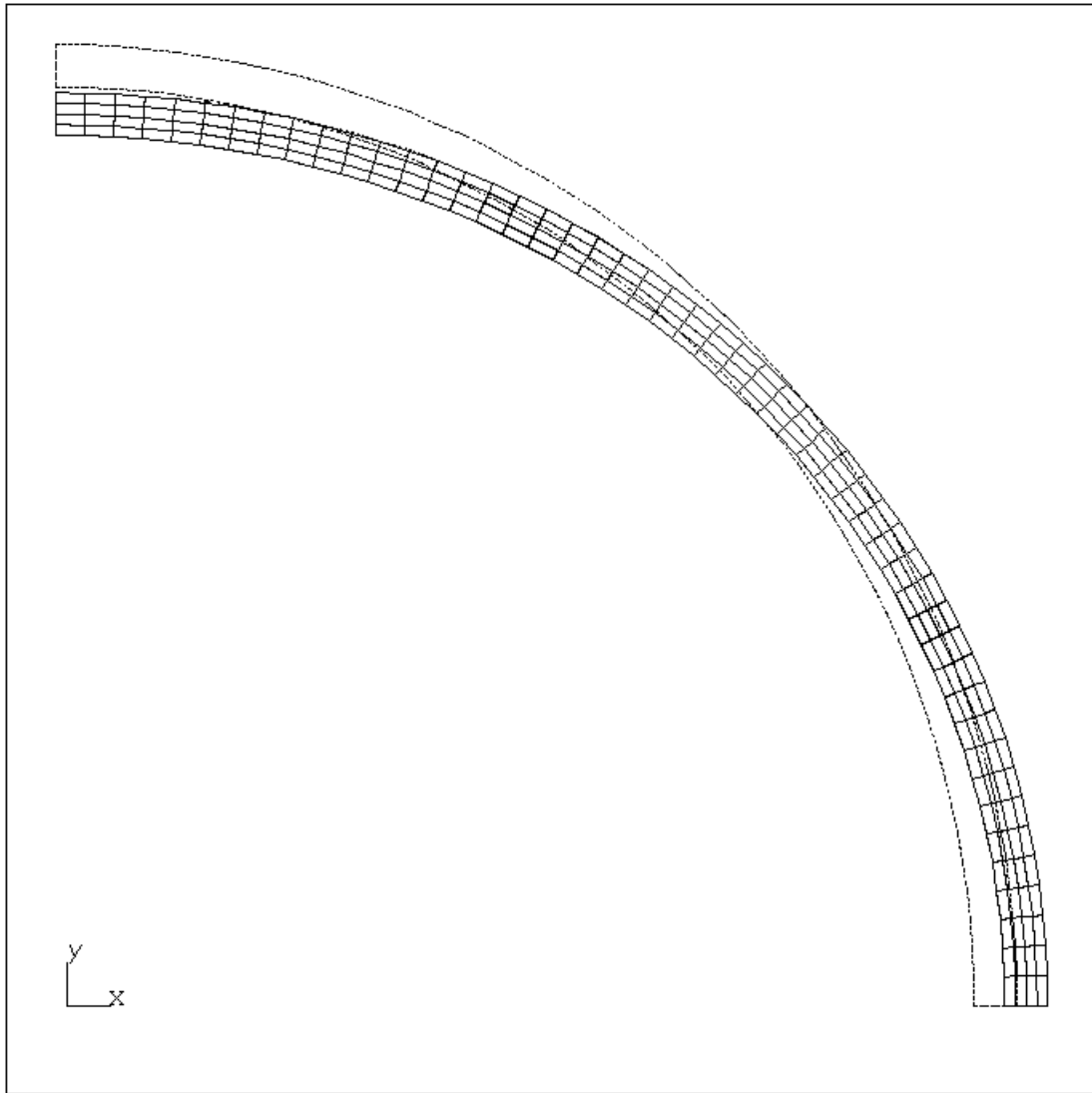


Figure 17: Deformed Shape and Meshing with Finite Element Analysis (Aluminum)

The displacements normalized by load in the radial and tangential directions according to the angle are shown in Figures 18 and 19. We see that the different compliances have the same shape but are not superposed, which means that the non-linearity created by the large deformations is important.

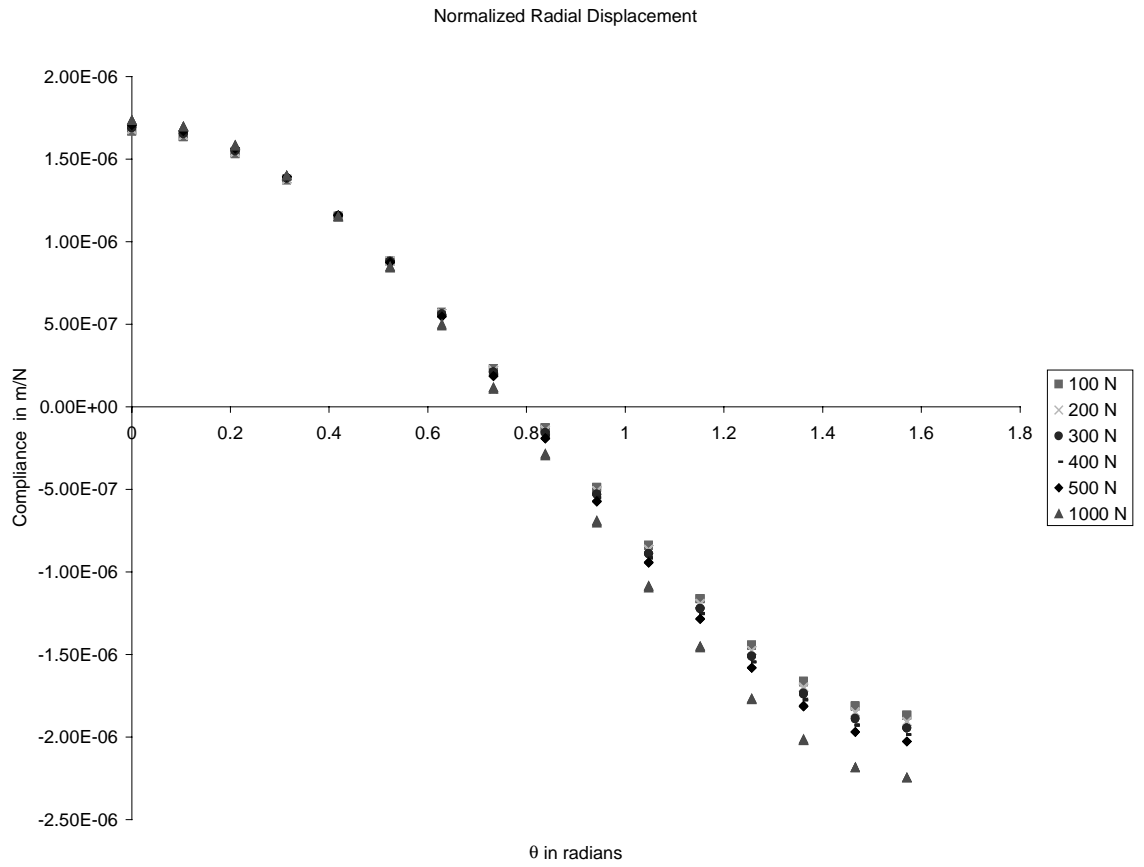


Figure 18: Normalized Radial Displacement from ANSYS Analysis

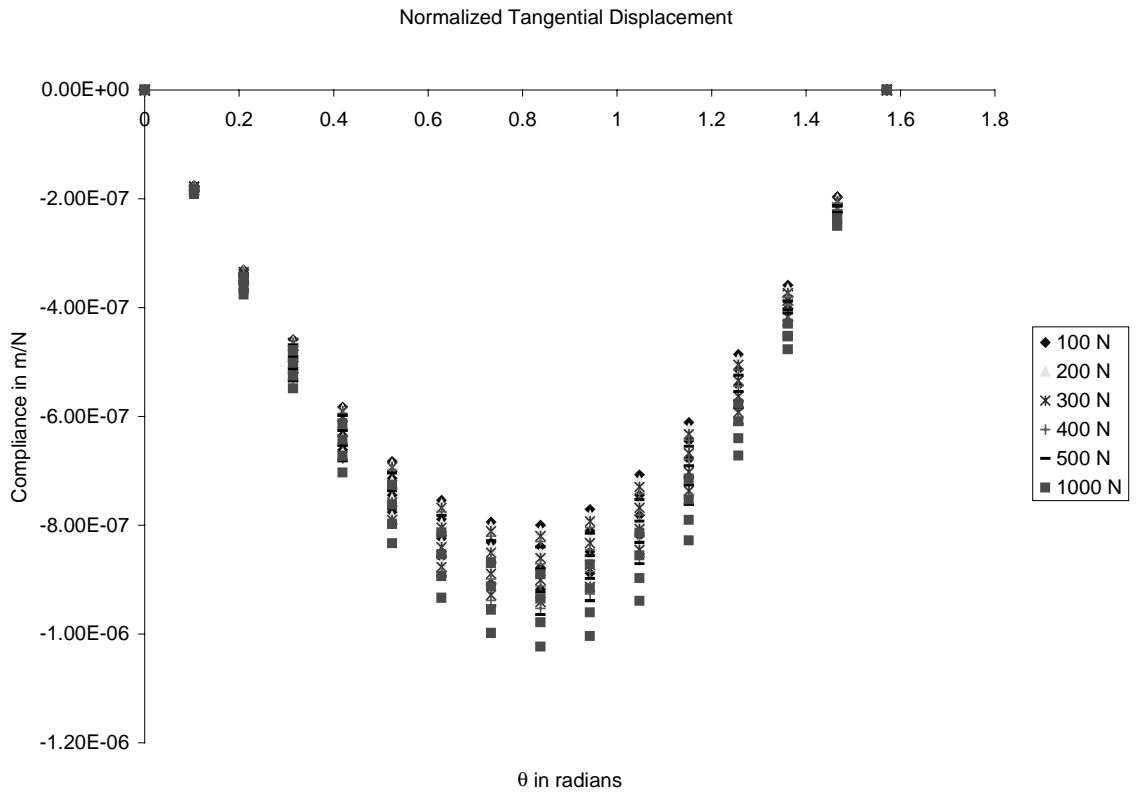


Figure 19: Normalized Tangential Displacement from ANSYS Analysis

The non-linear deflection prediction gives a result for the pipe stiffness 5% smaller than the experimental data for the aluminum ring at a load of 100 N. Furthermore, the theoretical strain is less than 1% of the experimental strain. In the case of the PVC ring, the theoretical deflection is 3.5% bigger. These differences are explained by the fact that the ratio of radius over thickness for this ring is 6.55 (less than 10 for the thin-wall theory), so the assumptions of the thin-wall theory are not respected. Therefore, using the plane strain modulus in our model (that is, taking into account the effects of Poisson's ratio due to the large thickness of the PVC ring), the theoretical deflection is now 2% smaller than the experimental value. We develop the non-linear solution in Chapter III.2.a.i taking into account the assumption of the elliptic deformed shape. The results show that the model remains valid for large deformation.

Table 6: Theoretical and Experimental Results for a 100 N Load

	Dy in m	Dx in m	Strain B %	Strain A %	Max Stress B Pa	Max Stress A Pa
PVC	0.000418					
Theoretical PVC	0.000424	0.000411				
FEM for PVC	0.000521	0.000467				
Aluminum	0.001210		0.108	0.208		
Theoretical Aluminum	0.001086	0.000997	0.106	0.189	$7.35 \cdot 10^7$	$1.31 \cdot 10^7$
FEM for Aluminum	0.000948	0.000868	0.0943	0.00162	$7.45 \cdot 10^7$	$1.30 \cdot 10^7$

III.1.b *Moisture Absorption Analysis*

Following Loos *et al.* [14], the pipe is assumed to be dry in its initial state. The moisture level on the inside of the pipe wall is held constant at a level corresponding to the saturation of the surface veil when immersed in water (0.036 kg/kg). Similarly, on the outside of the pipe wall a constant relative humidity of 50% is assumed and the corresponding saturation level is therefore 0.0042 kg/kg. These values have been taken from Loos's study.

A drop of water placed on the exposed edge of a section of the pipe material is absorbed rapidly by the sand reinforced polyester core. Hence, moisture transport through the core may be assumed to be instantaneous in relation to the absorption times of the other plies, and so the diffusion problem does not consider this layer. Therefore, only the surface veils, the liner, and the inner and outer skin are considered in order to evaluate the concentration profile across the pipe wall. The moisture concentration throughout the core is assumed to be constant at the level corresponding to the interface of the inner and outer skins in the diffusion problem.

Pritchard and Speake [20] report diffusion coefficients for a polyester resin reinforced unidirectional glass fiber laminate (weight fraction of glass is 48%) at 30° C. A linear interpolation based on the glass content is used to determine the diffusivity of each ply in the pipe. Ply diffusivities range from $1.32 \times 10^{-12} \text{ m}^2/\text{s}$ to $0.81 \times 10^{-12} \text{ m}^2/\text{s}$.

III.1.c *Life Prediction Analysis*

III.1.c.i **Failure Function and Remaining Time to Rupture**

The tests were performed on chopped strand mat laminate in air by Phillips [15]. The failure function described in Equation 1.2.13 (p. 19) is closely related to the data and the value of the materials under consideration. We choose to use these data for the remaining time to rupture in the lifetime prediction of the Owens Corning pipe, but we use other values for the remaining time to rupture of the hoop layers that we back calculated from Owens Corning pressure tests data. We use the following values in Equation 1.2.13:

$A = 19.4$ and $B = 20$ for all layers, except

$A = 20.202$ and $B = 20.202$ for the hoop layers.

We choose the above values according to existing data on E-glass reinforced polyester. For the hoop layers, we modified the values of A and B according to the pressure tests conducted on the studied pipe. The life prediction correspond to the experimental data if we allow this small change in the values of A and B .

III.1.c.ii Life Prediction Method

The life prediction is based on the model shown here in Figure 20.

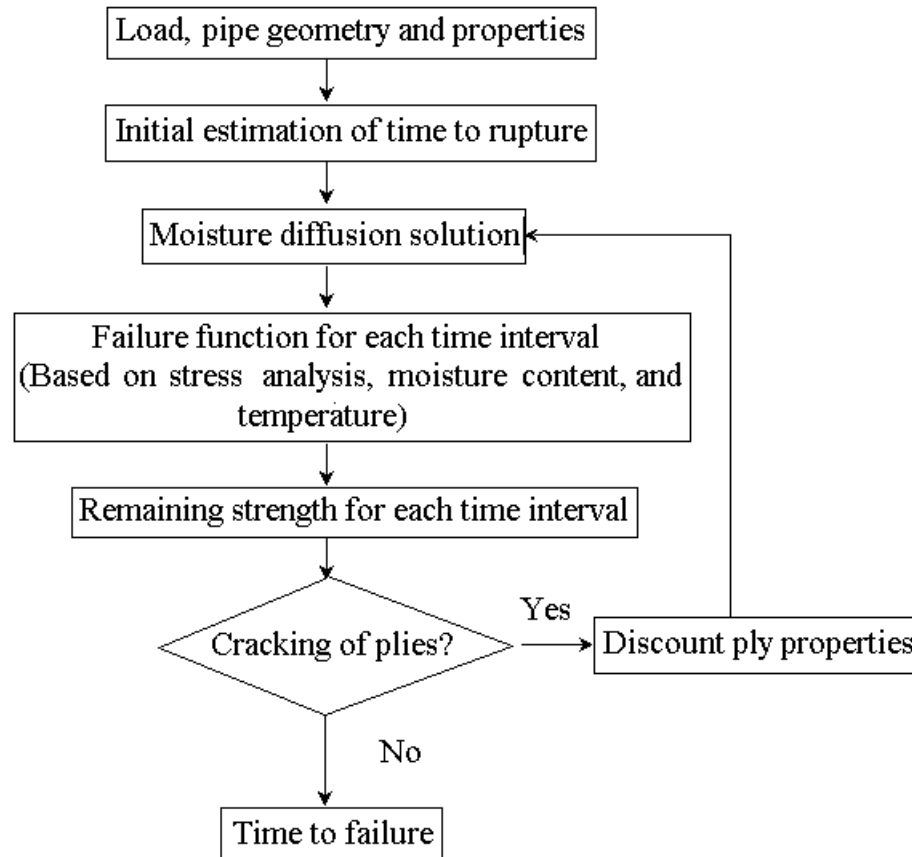


Figure 20: Diagram of the Life Prediction Code

A first stress analysis is done with every element of the problem; that is, the geometry, the type of load, and initial moisture and temperature. Using the maximum stress failure function Fa , and the remaining time to rupture function, a first estimation of the time to rupture is computed in order to estimate roughly the range of computation. This first estimation of time is then divided into several small steps whose size depends

on the required accuracy of prediction. The moisture is computed over each step of time of the total time using the Fickian moisture diffusion model detailed in Chapter I.2.b.ii.

A loading and temperature profile must be defined according to this time division. If the pipe is constrained with constant conditions other than moisture diffusion (such as surge pressure, water hammer, automobile and truck traffic cyclic loading, or temperature variation), the loading profile must be modified as a consequence.

Then, the failure function Fa and the remaining time to rupture are evaluated for each interval of time according to the corresponding constraint and the corresponding reduced material properties due to moisture content. Using the previous data and the method developed later in Chapter III.2.c, the remaining strength is computed for each ply of the laminate at each interval.

The failure occurs when the failure function Fa becomes bigger than the remaining strength. Once a ply fails, the properties of the ply are reduced to 10% of their original value. The new values of Fa are computed again with the new reduced material properties and the same loading profile. The moisture content must be computed again in a new geometry, which now includes a cracked ply. Then the remaining strength and the time to failure are computed again. This procedure is repeated until all plies fail.

III.2 **Models**

III.2.a *Stress Analysis*

Integrated in the life prediction code is the elasticity solution for the cases of internal pressure and axial load. The stresses are determined for each ply with any level of moisture and temperature according to the materials properties and the load. A bending stress analysis model is also developed to complete the stress analysis of service loading.

III.2.a.i **Bending Model**

The complex loads of soil pressure and driveway periodic load have been studied in detail, and Eckstein [21] and the AWWA [5] have defined a closed-form equivalent of two point-bending loads. We use this model approximate the real in-service loading conditions.

To establish a correct bending stress analysis, we will first develop an analysis for an isotropic material. By using the model indicated in the paragraph above, we simplify loading for this study as point forces on both the top and bottom of the pipe (see point A in Figure 11, p. 37).

To begin, we describe the deformed shape of an isotropic hollow cylinder under such a load. The results discussed in Chapter III.1.a show that the pipe keeps a shape that is approximately elliptical as long as the stresses are in the elastic range of the material.

Because the ratio of the pipe thickness to its radius is very small, we can assume that the strains due to stretching in the pipe can be disregarded with respect to the bending strain. As a result, the length of the ring remains the same.

Using the studies on buried pipe presented in Buczala and Cassady [2] and Eckstein [21], a finite element code, and the previous statement, we build an approximate solution for the problem under consideration.

First, we must develop an approximate static solution for an isotropic material. The model is based on the large deformation assumption. The resultant force and bending moment are computed according to the deformed shape of the ring. Figure 21 shows the expression of the load in the pipe:

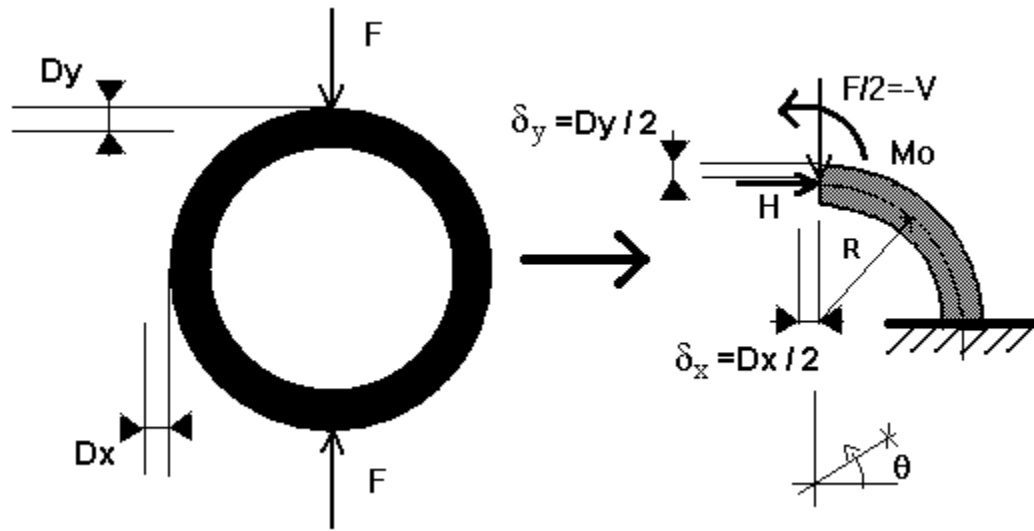


Figure 21: Model for Castigliano's Second Theorem

The strain energy in the ring is the following:

$$U = \frac{1}{2} \int \sigma \varepsilon dV \quad (3.2.1)$$

And, with the constitutive relation of an isotropic material and assuming there is only one nonzero stress component, we have:

$$U = \frac{1}{2} \int E \varepsilon^2 dV \quad (3.2.2)$$

The strain in the thickness has the following equation in which we assume that there is only bending in the ring during the transverse loading:

$$\varepsilon = z \kappa, \quad \text{and} \quad \kappa = \frac{M}{E I} \quad (3.2.3)$$

Thus, in the case of thin-walled theory, we have for the complementary flexural energy U after integration through the thickness and the length of the ring:

$$U = \frac{1}{2} \int_0^{\pi} \frac{M^2}{E I} R d\theta \quad (3.2.4)$$

The arc length of the deformed shape, ds , is considered here to be $Rd\theta$ as for the undeformed ring. As a result, the total arc length is equal to the total initial arc length of the ring. This approximation is made to eliminate the elliptic integral that results from considering the deformed arc length. The numerical evaluations of U with the elliptic arc length and of U with the circular arc length do not differ more than 5% for the large deformations we calculate for the aluminum ring up to 1000 N.

The resultant moment in the pipe thickness as a function of θ is the following (see Figure 21 above) according to δ_x and δ_y (the deflection in the x and y directions):

$$M(\theta) = V (R + \delta_x) \times \cos(\theta) + H (R - \delta_y) (1 - \sin(\theta)) + M_o \quad (3.2.5)$$

In this problem we consider that $H = 0$ because of the symmetry of the geometry. Thus, by substituting Equation 3.2.5 into Equation 3.2.4, we obtain the following:

$$U = \frac{1}{2} \int_0^{\frac{\pi}{2}} \frac{(V (R + \delta_x) \times \cos(\theta) + M_o)^2}{E I} R d\theta \quad (3.2.6)$$

Castigliano's second theorem gives the following equations for the deflection in y and the rotation at $\theta = \frac{\pi}{2}$:

$$\delta_y = \frac{\partial U}{\partial F} \quad , \quad \delta_y = - \frac{R \left((R + \delta_x) M_o + \frac{(R + \delta_x)^2 \pi V}{4} \right)}{E I} \quad (3.2.7)$$

$$\text{rotation } \theta = \frac{\partial U}{\partial M_o} \quad , \quad \text{rotation } \theta = \frac{R \left(M_o \frac{\pi}{2} + (R + \delta_x) V \right)}{E I} \quad (3.2.8)$$

The symmetry of the pipe geometry gives a rotation equal to zero at the top (point A on Figure 11, p. 37).

$$\text{rotation } \theta = 0 \tag{3.2.9}$$

Then, solving Equation 3.2.9 above, the moment M_o is defined as a function of V and H :

$$M_o = -\frac{-2(R + \delta_x)V}{\pi} \tag{3.2.10}$$

Replacing Equation 3.2.10 in 3.2.7 we obtain the general solution for a pipe with isotropic material in bending.

Eckstein [21] and the AWWA [5] give a way to approximate the vertical pipe stiffness (Load (N/m) per unit depth under vertical deflection); here we find the same results if we consider the case of the linear theory where $\delta_x = 0$ in the following equation:

$$\delta_y = \frac{V (R + \delta_x)^2 R}{E I} \left(\frac{\pi}{4} - \frac{2}{\pi} \right) \quad (3.2.11)$$

where R is the radius to the centroid of the cross section, E is the stiffness of the material, and I is the bending modulus given by the following equation:

$$I = \frac{l t^3}{12} \quad \text{and} \quad \hat{E} = \frac{E}{(1 - \nu^2)} \quad \text{for plane strain "modulus"} \quad (3.2.12)$$

Here, l is the length of the pipe, t is the thickness of the pipe wall, and ν is Poisson's ratio of the material.

In the case of a composite material, the corresponding value of EI is the inverse of the first element of the fully inverted bending stiffness matrix (Jones [22]) in the classical laminate theory.

Equation 3.2.11 has two unknowns, δ_x and δ_y , but using the bending without stretching assumption, the conservation of the arc length of the ellipse gives Equation 3.2.13, allowing us to solve this non-linear problem.

$$s = \int_0^{2\pi} \sqrt{(R + \delta_x)^2 \cos(\theta)^2 + (R - \delta_y)^2 \sin(\theta)^2} d\theta = 2 \pi R \quad (3.2.13)$$

The integral can be approximated by the following equation, which is easier to solve numerically as long as the total deflection is less than 60% of the diameter:

$$s = ((R + \delta_x) + (R - \delta_y)) \left(1 + \frac{3 \left(\frac{(R + \delta_x) - (R - \delta_y)}{(R + \delta_x) + (R - \delta_y)} \right)^2}{10 + \sqrt{4 - 3 \left(\frac{(R + \delta_x) - (R - \delta_y)}{(R + \delta_x) + (R - \delta_y)} \right)^2}} \right) \quad (3.2.14)$$

By incrementing an initial δ_x given by the linear theory and computing the corresponding δ_y for the ellipse with Equation 3.2.14 above, we find the solution corresponding to the minimum value of the difference between the previous δ_y and the one given by Equation 3.2.11.

Using the same bending without stretching theory, the mechanics of a curved beam as presented by Luo and Sun [3] gives the same relation for the pipe stiffness, but we now have the moments on the edge and the top of the ring indicated by the following expressions in which F is the applied load and R is the mean radius:

Bending moment on the top:

$$M_a = -\frac{F\left(R + \frac{D_x}{2}\right)}{\pi} \quad (3.2.15)$$

Bending moment on the side:

$$M_b = -\left(\frac{1}{2} - \frac{1}{\pi}\right) F \left(R + \frac{D_x}{2}\right) \quad (3.2.16)$$

Now, if we consider the ratio of thickness over radius to be small enough (a value of 0.1 is the maximum), we can use the classical theory to compute the strain and the stresses in the materials at these two points. The resultant forces in the laminate reference for the classical laminate theory are:

$$\text{At point A: } N = \begin{pmatrix} 0 \\ 0 \\ 0 \end{pmatrix}, M = \begin{pmatrix} 0 \\ M_a / width \\ 0 \end{pmatrix} \quad (3.2.17)$$

$$\text{At point B: } N = \begin{pmatrix} 0 \\ -F / (2 * width) \\ 0 \end{pmatrix}, M = \begin{pmatrix} 0 \\ M_b / width \\ 0 \end{pmatrix} \quad (3.2.18)$$

The moments are divided by the width of the pipe because the bending matrix D does not integrate it.

We can compute the maximum strain using a beam theory. An approximation of the strain on the edge of the external side of the pipe is then:

$$\varepsilon_{\max} = \frac{M_b \frac{h}{2}}{E I} \quad (3.2.19)$$

The integration into Castigliano's second theorem of the elliptically deformed shape, gives the following value for the resultant moment M_b :

$$M_b = -\left(\frac{1}{2} - \frac{1}{\pi}\right) F \left(R + \frac{D_x}{2}\right) \quad (3.2.20)$$

where D_x is the deflection. Thus, replacing Equations 3.2.20 in 3.2.19, we obtain the following:

$$\varepsilon_{\max} = \frac{-\left(\frac{1}{2} - \frac{1}{\pi}\right) F \left(R + \frac{D_x}{2}\right) \frac{h}{2}}{E I} \quad (3.2.21)$$

Rearranging Equation 3.2.21 with the total deflection Equation 3.2.11 we have:

$$\epsilon_{\max} = \frac{-\left(\frac{1}{2} - \frac{1}{\pi}\right)\left(\frac{\pi}{4} - \frac{2}{\pi}\right)^{-1} 4 h D_y}{\left(D + \frac{D_x}{2}\right)^2} \quad (3.2.22)$$

The numerical result is the following, which is the same formula used in the ring bending tests ASTM standard D3681 if we consider that D_x is almost the same as D_y :

$$\epsilon_{\max} = \frac{4.8848 h D_y}{\left(D + \frac{D_y}{2}\right)^2} \quad (3.2.23)$$

This result agrees with research conducted by Pearson [9]. We can therefore assume that this model is valid for Owens Corning composite pipes. Using Equation 3.2.19 above, we find results which agree closely with the experiments shown in Figure 15 (p. 41).

III.2.a.ii Superposition of Bending and Pressure Model

We assume that the two stress analyses we developed can be superposed because the pressure creates primarily hoop stress, while the transverse load creates bending in the pipe wall resulting in stress in the hoop direction as well.

In the model, in order to obtain the strain and the stresses in the plies, we superpose the bending stress due to transverse load and the hoop stress due to pressure. Because hoop stress is the major stress in both cases, this last statement is compatible with the maximum stress failure criterion we use for life prediction from the point of view of failure function.

Even if we combine a linear solution and a non-linear solution, we assume that the combined effect of pressure and transverse load makes the stress change because the pressure pushes on the wall of the pipe and tends to round the elliptical shape due to the transverse load. Then, the deflection is reduced as the internal pressure makes the pipe more round and reduces the bending stress. It is important to keep in mind that the prediction needs to be as accurate as possible but still conservative with respect to the real material behavior.

The moisture and the temperature create environmental stresses due to the expansional strains detailed previously. Those stresses are not included in the bending model because they have already been incorporated into the axial-symmetric solution.

III.2.b *Moisture Absorption Model*

Loos *et al.*, [14] observe that the diffusion characteristics of polymeric composites are generally not Fickian, although, as previously mentioned, the differences with the

Fickian model are admissible at room temperature. In order to simplify treatment of this problem, a simple Fickian diffusion assumption is made. Furthermore, since the pipe wall thickness is approximately 1-2% of the nominal pipe diameter, a one-dimensional diffusion model is used.

A finite difference scheme is used to solve for the concentration profile within the pipe as a function of time.

However, further research must be done to determine the moisture absorption after the apparent moisture saturation, taking into account the damage level of the composite due to swelling stresses and cracking.

III.2.c *Life Prediction Model*

The life prediction analysis is based on damage accumulation. We need to estimate the remaining strength of the laminate during long-term loading. To do so, we make use of the idea of a *characteristic damage state* (see Reifsnider and Stinchomb [23]). This idea suggests that the final damage state during fatigue is identical to the final damage state during quasi-static loading. This concept has been developed for matrix cracking accumulation and it has been extended in the current solution to include fiber cracking accumulation.

The failure function is the damaged state of the composite under a given state of stresses at a given time. For our life prediction code, we use the following function (a maximum stress criterion):

$$\text{If } \sigma_{\theta\theta}^i \geq 0 \text{ then } Fa = \frac{\sigma_{\theta\theta}^i}{Xt_i}; \text{ if not, then } Fa = -\frac{\sigma_{\theta\theta}^i}{Xc_i} \quad (3.2.24)$$

The failure function is applied to every layer of the pipe. The stresses in each of the pipe layers change with the moisture content and damage. The life prediction determines which plies fail in order to discount the material properties in the stress analysis and the diffusion analysis. In the present code, we predict burst failure. The pipe bursts when the glass fiber of the hoop glass layers fails. The burst failure mode requires the use of the maximum stress failure function in the fiber direction. The failure function is selected according to the expected type of damage.

We use this failure function to estimate the time to rupture for a given constant Fa_i on a given interval i . The time to rupture is taken as a result of the failure function value on this interval.

$$t_{rupture}(Fa_i) = 10^{\frac{Fa_i - A}{B}} \quad (3.2.25)$$

In the above equation, A and B are material parameters determined with the classical $S-N$ curve for the same failure mode. These curves are experimentally obtained by performing static tests. Time to rupture is recorded versus given stress. In the case of maximum stress criteria, Fa (stress of the test divided by strength) is recorded versus time to rupture.

The remaining strength function equation according to Reifsnider and Stinchomb [23] is written as follows:

$$Fr = 1 - \int_0^{\tau} (1 - Fa(\tau)) j \tau^{j-1} d\tau \quad (3.2.26)$$

We estimate the value of Fa at a discrete value in time, so we will integrate this equation easily. The failure function, Fa , is considered to be constant over the interval of integration. Thus, the change in the remaining strength over the interval i is equal to:

$$\Delta Fr = Fr(\tau_{i+1}) - Fr(\tau_i) = -(1 - Fa)(\tau_{i+1}^j - \tau_i^j) \quad (3.2.27)$$

where ΔFr is the change in remaining strength over the interval and τ_i is the normalized time expressed at a discrete point. The normalized time for the rupture condition is expressed as follows:

$$\tau = \frac{t}{t_{rupture}} \quad (3.2.28)$$

For the first interval we can evaluate Fr_1 as a function of Fa , time of the interval and time to rupture, because at $\tau_0 = 0$ we have remaining strength equal to 1.

$$Fr_1 = 1 - (1 - Fa_1) \left(\frac{t_1}{t_{rupture}(Fa_1)} \right)^j \quad (3.2.29)$$

Using Equations 3.2.27 and 3.2.29 above we have the following for τ_2 :

$$\tau_2 = \left(\frac{1 - Fr_1}{1 - Fa_2} \right)^{1/j} \quad \text{and} \quad t_2^0 = \left(\frac{1 - Fr_1}{1 - Fa_2} \right)^{1/j} * t_{rupture_2} \quad (3.2.30)$$

In the above, t_2^0 is the equivalent of pseudo-time corresponding to the same time necessary to reach the same remaining strength with the same Fa for this interval. Fa is computed with the real time of this interval. In the next step, t_2^0 takes into account the previous accumulation of damage, giving a calculation for the following step starting at $t = t_2^0$. We use Equation 3.2.25 (p. 64) to calculate $t_{rupture_2}$.

The pseudo-time is important in this theory because the damage in the laminae is considered to occur uniformly before rupture. According to Reifsnider and Stinchomb

[23], the fatigue damage processes are non-conservative processes and the current state of the material is dependent on the history of prior loading and associated deformation. The damage level is taken to be proportional to the density of micro-cracks and failure is considered as saturation of the crack density. The damage level increases in time according to the failure function and the state of damage level itself, and t_2^0 takes into account the previous state of damage.

With Equation 3.2.27 (p. 65) we can compute the remaining strength on the next interval of time.

$$\Delta Fr = Fr_2 - Fr_1 = -(1 - Fa_2) \left(\left(\frac{t_2^0 + \Delta t}{t_{rupture_2}} \right)^j - \left(\frac{t_2^0}{t_{rupture_2}} \right)^j \right) \quad (3.2.31)$$

where

$$\Delta t = t_2 - t_1 \quad (3.2.32)$$

By repeating this process, we can calculate Fr (the remaining strength in terms of the selected failure function) for each interval. The predicted lifetime is then calculated to be the time at which the values of Fr and Fa are equal.

IV RESULTS AND C ONCLUSIONS

IV.1 Results of Calculations

IV.1.a Results for Burst Pressure Life Prediction

Figure 22 shows the Owens Corning test results of time to failure along with the prediction from the remaining strength analysis. The time to failure corresponding to the lowest initial strain level of 0.682% is used to establish the relation between the stress rupture time and the failure function value for the inner and outer skin as given by Equation 1.2.13 (p. 19).

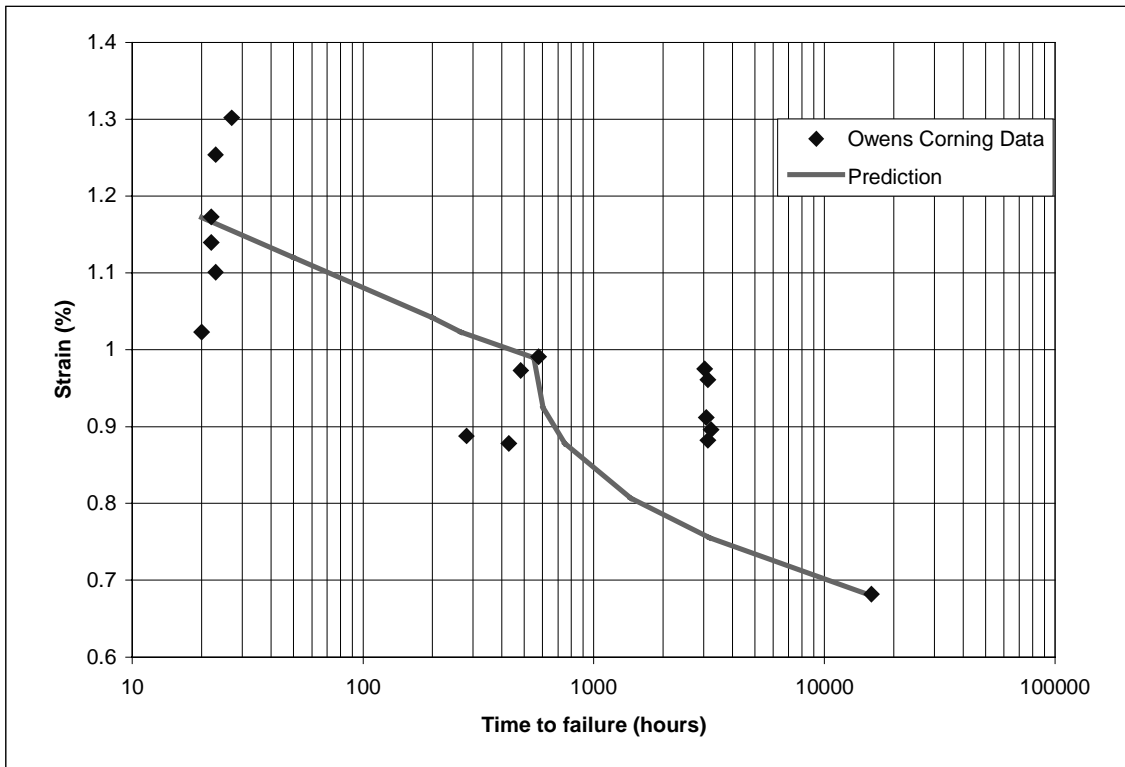


Figure 22: Burst Pressure Test at Room Temperature for 600 mm Diameter Flowrite Pressure Pipe: Data, Prediction

The moisture attains equilibrium within the pipe wall at approximately 2750 hours (115 days). For pressures greater than 34 bar, matrix cracking of the core is predicted to occur within 8 hours; hence, the hoop stiffness and the shear stiffness of the core are discounted to half of their respective initial values at the start of the remaining strength evaluation. For pressure levels below 34 bar, the outer skin is the first ply to fail; therefore, no discounting of ply properties is done prior to or during remaining strength evaluation. Since the core is not considered in the diffusion problem, the calculation of moisture concentration is unaffected at all pressure levels considered.

Examples of the remaining strength and failure function evolution with time for the outer skin are shown in Figures 23, 24, 25, and 26. Figures 23 and 24 correspond to an internal pressure of 45 and 38.05 bar and an initial strain of 1.172% and 0.991%, respectively. Failure for the two cases is predicted at approximately 34 and 340 hours. In both cases, the remaining strength curve shows a “sudden death” trend and the failure functions also increase noticeably with time. This is because the moisture has not yet reached equilibrium and there is a stress redistribution in the pipe wall as a result of a decrease in the stiffness of the other plies. The failure function also increases because of the decrease in strength of the outer skin due to the increasing moisture content.

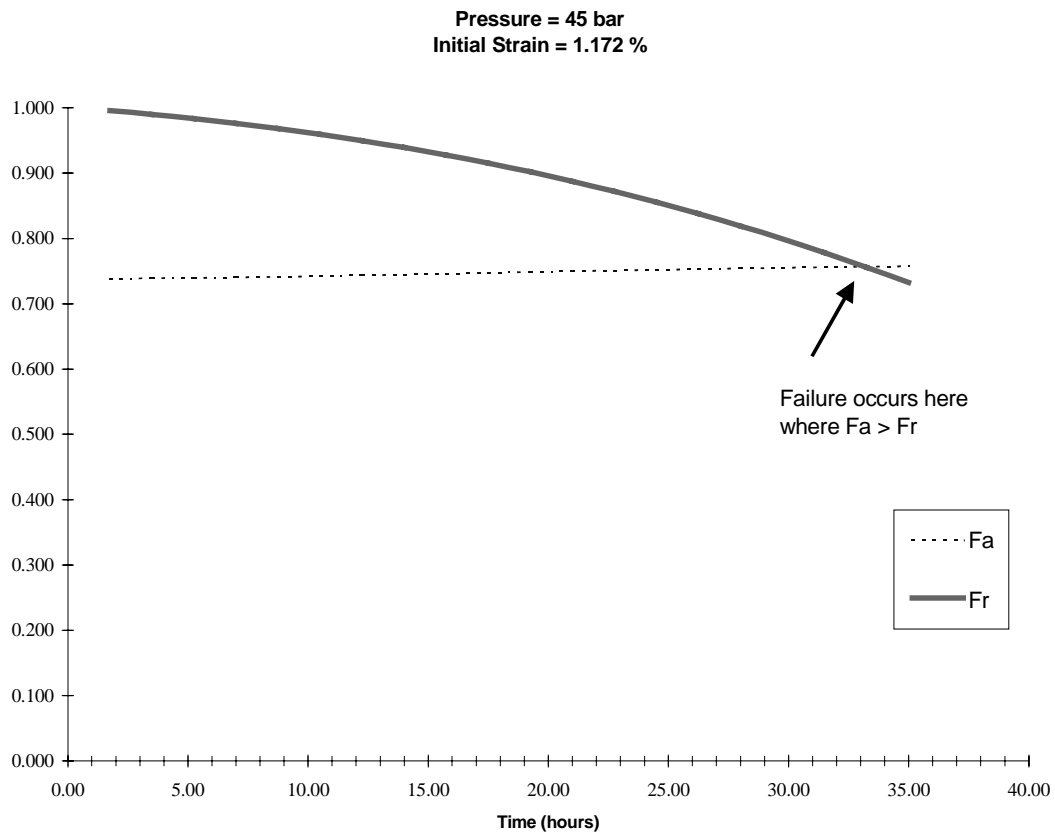


Figure 23: F_a and F_r Functions versus Time for an Initial Hoop Strain of 1.172% (45 bar)

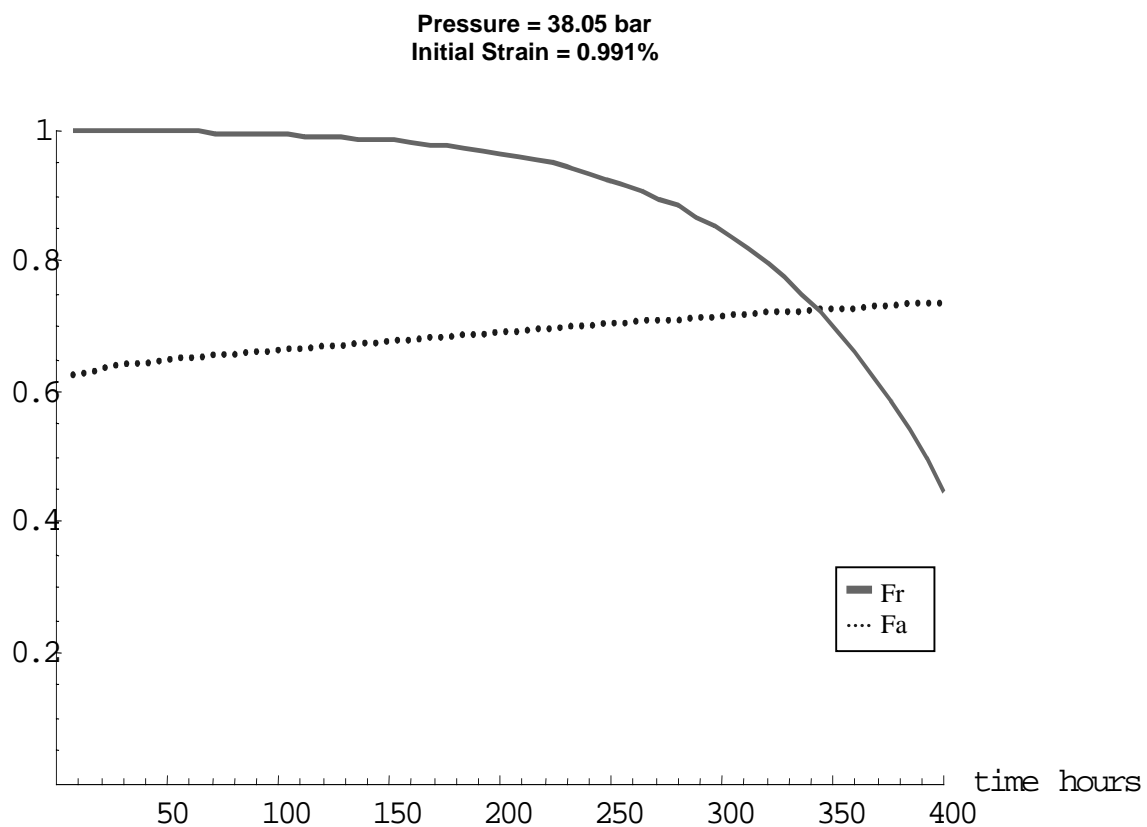


Figure 24: F_a and F_r Functions versus Time for an Initial Hoop Strain of 0.991% (35.08 bar)

Figure 25 shows remaining strength and failure function curves for the outer skin at an internal pressure of 35.5 bar and an initial strain of 0.925%. Failure is predicted at 570 hours. Once again the “sudden death” trend in the remaining strength curve is noticeable.

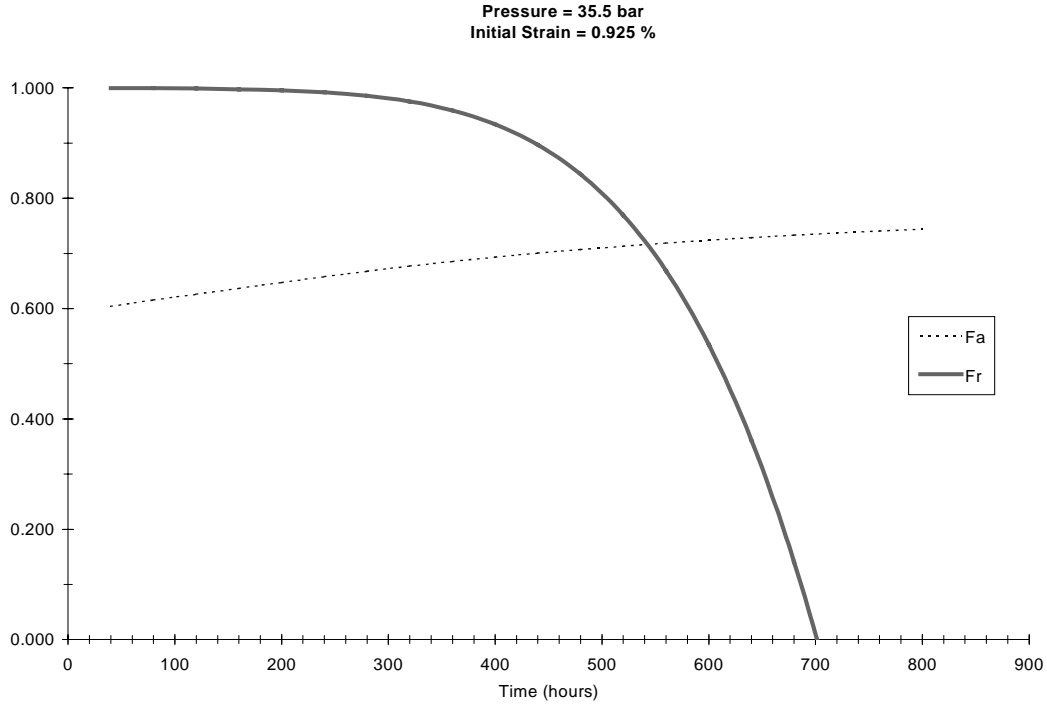


Figure 25: F_a and F_r Functions versus Time for an Initial Hoop Strain of 0.925% (35.5 bar)

The remaining strength and failure function evolution for an internal pressure of 26.19 bar and an initial strain of 0.628% is shown in Figure 26. As expected, the failure function is almost constant after the moisture level saturates at approximately 2750 hours, after which time the remaining strength curve is linear. The stress rupture time for the inner and outer skin given by Equation 1.2.13 (p. 19) is determined based on the time to failure at this pressure level.

Pressure = 26.19 bar
Initial Strain = 0.682 %

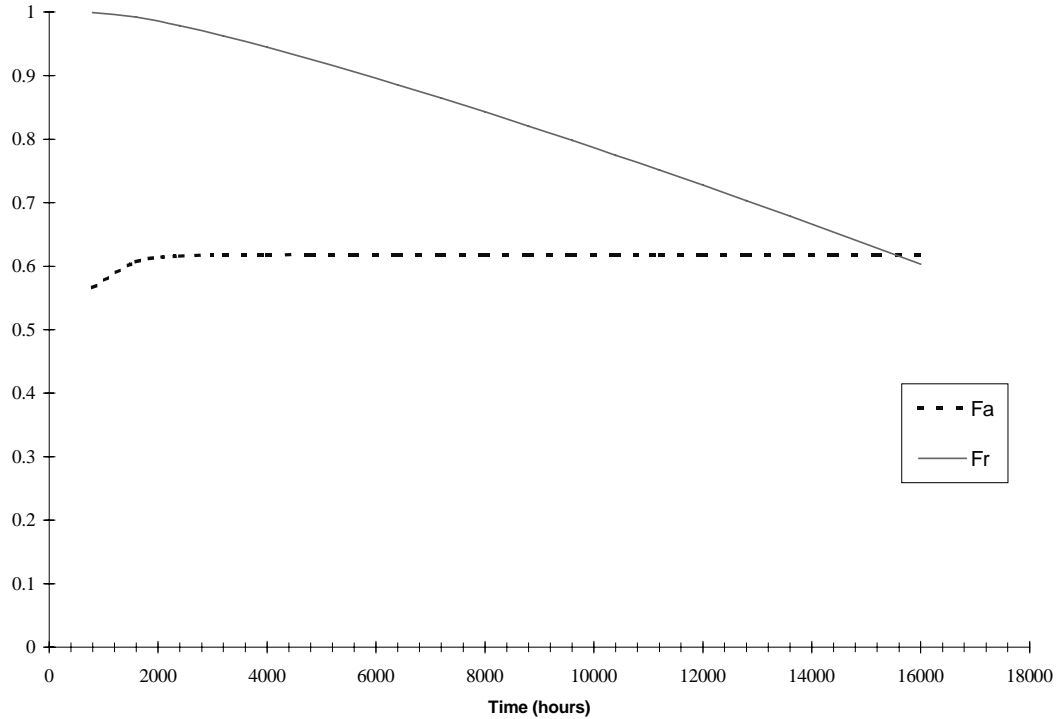


Figure 26: *Fa* and *Fr* Functions versus Time for an Initial Hoop Strain of 0.682% (26.19 bar)

It is interesting to note that for pressures below 34 bar no matrix cracking is predicted to occur in the core. In fact, the failure function actually decreases with time. Since the stiffness of the core is lower than that of the other plies, the core does not contribute to containing the hoop forces in the pipe walls. Hence, the moisture level in the pipe wall significantly influences the hoop stresses in the core. Initially, the core is dry and the hoop stresses in the core are tensile. As the moisture level increases, the

hoop stresses in the core change from tension to compression, especially since there is no swelling in the hoop direction for the adjacent layers (hoop wound glass). When the hoop stresses in the core are compressive, the maximum stress criterion uses the compressive strength of the core material, which is greater than the tensile strength. These factors combine to produce a failure function for the core, which decreases with time and then remains constant at a value less than the initial value.

IV.1.b Results for Ring Bending Life Prediction

The results of life prediction for the ring bending test are shown in Figure 27. We use the same time to rupture function as in the pressure test because the prediction in the case of the pressure test is consistent with the data. The experimental data shown in Figure 27 below are from Pearson [13].

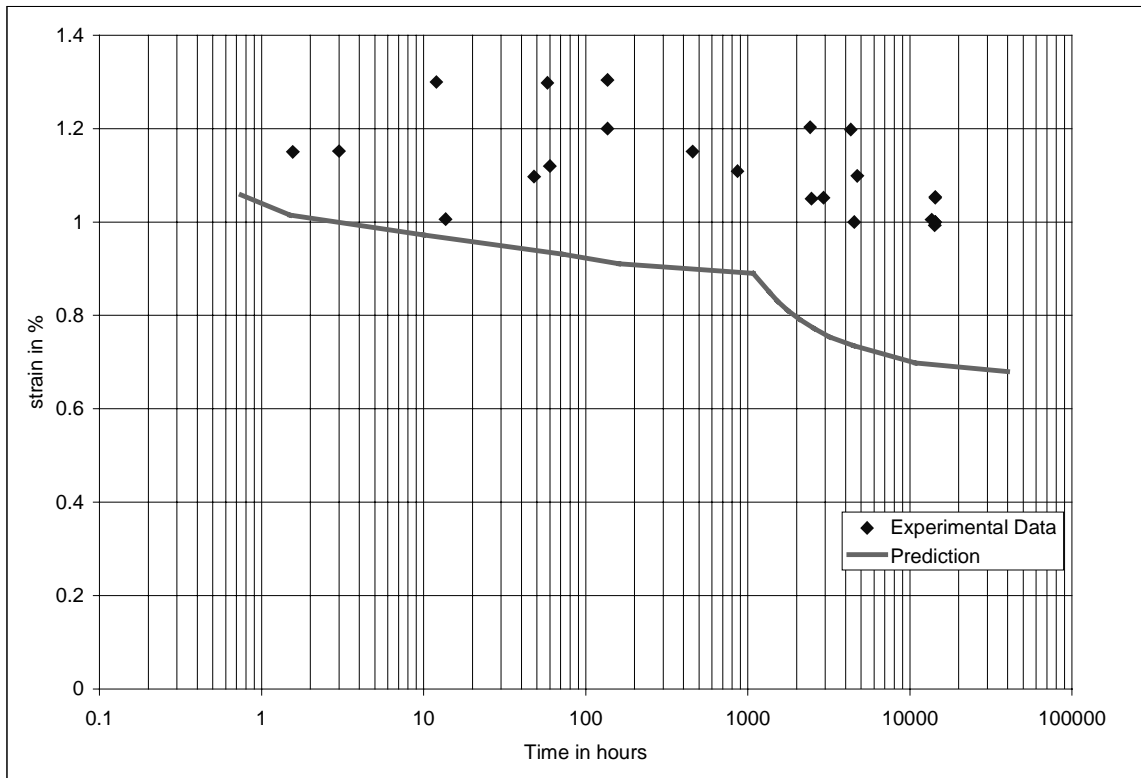


Figure 27: Ring Bending Test at Room Temperature for 600 mm Diameter Flowrite in Acid Environment: Data, Prediction

The tests were performed on the same Flowrite Pipe as the one we used for our model. The tests consist of exposing the interior of pipe to a 5% sulfuric acid fluid.

The stress analysis shows that the bending at the top of the ring is initially close to twice the bending at the side. If the ring does not fail immediately at the top, there will be failure at the side. This is true because moisture diffusion creates compression stresses in the inside layers due to swelling, and it also creates tensile stresses in the external layers because of the equilibrium in the bending of the pipe. The stresses at the top and bottom are in tension in the internal layers and in compression in the external

layers; however, the moisture diffusion tends to relax these stresses. It is the inverse on the sides of the pipe, where the moisture tends to increase the stresses; thus it is here that the failure occurs. The life prediction shows two types of first failure: first failure at the top and bottom of the pipe, and first failure at the sides of the pipe. As we notice in the results of the life prediction, at high transverse load the pipe fails after a very short time. This short time does not allow the moisture to diffuse and to relax the stresses as previously mentioned, so the failure should occur where the stresses are initially greater; that is, at the top and the bottom. At a lower load, the loading stresses are not sufficient to cause failure of a ply. The moisture increases with time and makes the stresses decrease at the top and bottom and increase at the sides. With a transverse load of less than a certain value, the first crack occurs in the sides. In the life prediction, this minimum transverse load is 29000 N/m (0.89% hoop strain).

The “jumps” and changes of curvature in the life prediction graphics show the typical change of failure mode due to the ply discount model. A failure in a ply can initiate the immediate failure of other plies and create the sudden death of the pipe. It can also relax stresses in certain plies by increasing stresses in others. When computing the lifetime at different loads, the leading mode of failure may change from one ply to another. At a load bigger than 29000 N/m (0.89% hoop strain), the first ply to fail is the inner skin at the top and bottom of the pipe which makes every other layer fail causes catastrophic failure. At a lower load, the failure occurs first in the filler and it changes the failure mode. At a load less than or equal to 29000 N/m, the first four plies crack

simultaneously, and, when the last ply (outer skin) cracks, the deflection induced is bigger than 60% which is beyond the limit allowed by our model. Thus, we consider the pipe failed in that case. At a load less than 26500 N/m the last ply to fail before catastrophic failure is the outer skin.

We stated in Chapter IV.1.a that the moisture reaches a saturation level at around 2700 hours. We can notice that the lifetime of the pipe does not increase noticeably with a lower load at a predicted time to failure of 2000 hours or less. Once the saturation level is reached, even if there are cracks in the laminate, the moisture does not change. The failure function remains constant and the remaining strength decreases according to the constant failure function as in creep fatigue.

In Chapter II.3.a we claim that the failure occurs locally in the pipe. In the code, when a ply fails the properties of the entire ply are discounted. In a real situation, the properties should be discounted only locally and a new stress analysis should be done taking into account the new geometry and the new properties. In most of the experimental data, the failure occurs when the pipe leaks or when the slope of deflection versus time increases to more than 0.25 (Chapter I.2.a.i). Before the first ply failure occurs, the stress analysis remains valid and, we can assume that when failure occurs at the top and bottom or in the sides of the pipe, the deflection in the real case changes dramatically. The first ply to fail can then be identified as a failure criterion of the pipe.

We must keep in mind that if one ply fails locally, the rest of the ply remains intact. However, in the model, the properties of the ply are now discounted and the stresses are redistributed to all the other layers of the ring. The new calculated stresses are bigger than those in the real case, and we will therefore underestimate the time to failure of the next ply. This fact allows us to claim that the model in which we discount the properties of failed plies is valid for our purposes but more experiments must be done to completely validate it.

The life prediction code gives the first failure at a load creating 30% deflection of the diameter. This requires the use of a non-linear model for large deflections. For short time life prediction, the stress analysis is still valid; the most important life predictions are needed for small deflections to lifetime predictions over 50 years.

However, the life predictions in the case of ring bending are a significantly shorter than expected and do not agree at all with the tests performed with acid water (a worse case than the case we tried to predict due to chemical effects). The tests were conducted at constant deflection and the predictions calculated at constant load. In any case, the loading during service is more similar to constant load than to constant deflection because the weight of a given amount of soil on the pipe does not change even if the soil is more compacted.

Several elements of the code may be changed for the results to more accurately reflect the data. The failure function has been chosen here to be maximum stress for every ply; but, for example, the polynomial failure criterion presented by Tsai and Wu [24] could have been used for the failure function of the hoop layers because it takes into account not only the hoop stresses, but also all other stresses, and can thus predict eventual matrix cracking before predicting fiber cracking.

We arbitrarily reduce to 50% the stiffness of the cracked ply in the discount process, but the exact values have not been investigated due to lack of material to be tested. If the discount coefficients are different for each ply due to the mode of failure, the life predictions might change significantly.

The tensile tests performed in the axial direction of the pipe (Figure 7 on p. 25 and Figure 8 on p. 26), show that even if the samples break at the predicted load, there is a stiffness reduction occurring at 50% of this load where any failure is predicted. In that case, the ultimate strength of the material evaluated according to the maximum stress criterion and that evaluated according to the Tsai-Wu polynomial failure criterion are close. The conclusions of those tests show that the choice of the failure function does not matter in that case, but the strength values we use are not correct and must be better investigated in further research.

Most of the data we use in the code have been provided by Owens Corning. But data such as diffusivity, remaining time to rupture function, corrosive resistance ability, and failure mode, all of which are major factors in the life prediction model, have been estimated according to similar works and research found in the literature.

IV.2 Conclusions and Directions for Future Research

We have developed a method of predicting the lifetime of composite sewage pipe subjected to load, moisture, and temperature. Several tests were performed by Owens Corning on such pipes. In our code we applied conditions identical to those in the Owens Corning tests.

The results agree with the data for the pressure tests, and show coherent and consistent behavior in the ring bending tests. The lack of specific data on polyester reinforced E-glass (diffusivity, accurate time to failure for our material configuration, and material property changes with aggressive environment) does not allow us to reach a solution approximating the existing data for the ring bending case.

However, using the appropriate data entries the present method is capable of taking into account varying loads and pressure profiles, varying temperatures, and moisture diffusion in the estimation of the lifetime of the pipe. The precision of the results depends on the magnitude of step of time interval we choose, as well as on the

accuracy of the inputs. The assumption of constant failure function over each interval of step time must remain valid and must converge to a solution when the step interval decreases.

The present method tends to underestimate the real lifetime of the product. In the ring bending test, the local failure is considered to be failure of the totality of the ply, and the ply properties are discounted for the whole pipe. The discount of the material properties should be further investigated because the failure of a ply does not mean that the ply no longer holds loads. In the code, we use an estimated discount factor of 50%, although this percentage is not accurate for all plies.

Because of the general property discount, the calculation of stress redistribution is not accurate. In future research, a finite element model for stress analysis could be constructed to better evaluate the real stress redistribution in the pipe after failure of a ply. A potential solution is to divide the ring into n small elements. In this solution we would consider each element as a partial annulus with a circular shape. We could then apply Castigliano's second theorem to each element with the same boundary conditions for two adjacent elements and the same no-rotation boundary conditions for the first and last elements. Then we would solve the solution with the appropriate material property discount for the element under consideration. This solution should take into account the large deformation geometry and the local failure for the stress analysis.

An accurate estimate of the stress rupture time for the different materials of the plies in environmental conditions is essential to accurate life predictions. One possibility is to use the test results for smaller times to failure of the pipe to more accurately determine the initial strength, and also to estimate the time to failure as a function of the failure function. At shorter times, the layers are relatively free of any moisture, and the time to failure of the pipe may be used to estimate the coefficients in the stress rupture equation for the critical elements under dry conditions. Such a relation may be used in conjunction with the effect of moisture on strength in the remaining strength calculation. It would also be more appealing to predict the long-term performance of the pipe from short-term data, rather than the short-term from the long-term.

The diffusion model must be improved because it needs to be more stable. The actual model requires a minimum time step for the computation of the moisture through time. The actual code does not allow the diffusivity of a ply to increase noticeably when it is failed. The Fickian model should be upgraded to a more accurate model for composites.

The specific material of a given pipe can have different remaining times to rupture compared to the data currently found in the literature. The changes in the remaining time to rupture according to the different environments should also be investigated. Other failure criteria have not been investigated in the present work, but would be worth investigation in future research.

The effect of water at elevated temperatures on the life of the pipe may also be a consideration for future research in diffusion, change in properties, and change in time to failure.

REFERENCES

- [1] Frost, S. R., and A. Cervenka, "Glass Fibre-Reinforced Epoxy Matrix Filament-Wound Pipes for use in the Oil Industry," *Composites Manufacturing*, No. 2, pp. 73-81, 1994.
- [2] Buczala, G. S., and M. J. Cassady, eds., *Buried Plastic Pipe Technology*, ASTM STP 1093, American Society for Testing and Materials, 1990.
- [3] Luo, J., and C. T. Sun, "Global-Local Methods for Thermo-elastic Stress Analysis of Thick Fiber-Wound Cylinders," *Journal of Composite Materials*, Vol. 25, pp. 453-463, 1991.
- [4] Hyer, M. W., and C. Q. Rousseau, "Thermally-Induced Stresses and Deformation in Angle-Ply Composite Tubes," *Journal of Composite Materials*, Vol. 21, No. 5, pp. 454-480, 1987.
- [5] American Water Works Association, "Chapter 5: Buried Pipe Design," *The AWWA Manual*, pp. 35-55.
- [6] Pagano, N. J., "Pure Bending of Helical Wound Composite Cylinders," *Analysis of the Test Methods for High Modulus Fibers and Composites*, ASTM STP 521, American Society for Testing and Materials, pp. 255-263, 1973.
- [7] Fuchs, H. P., and M. W. Hyer, "Bending Response of Thin-Walled Laminated Composite Cylinders," *Composite Structures* 22, pp. 87-107, 1992.

- [8] Claydon, P., G. Cook, P. A. Brown, and R. Chandwani, "A Theoretical Approach to Prediction of Service Life of Unbonded Flexible Pipes under Dynamic Loading Conditions," *Marine Structures* 5, pp. 399-429, 1992.
- [9] Pearson, L. E., "Fiberglass Pipe Product Standards -- An Update on Performance," in Buczala and Cassady, eds., *Buried Plastic Pipe Technology*, ASTM STP 1093, American Society for Testing and Materials, pp. 40-56, 1990.
- [10] Mruk, S. A., "The Durability of Polyethylene Piping," in Buczala and Cassady, eds., *Buried Plastic Pipe Technology*, ASTM STP 1093, American Society for Testing and Materials, pp. 21-39, 1990.
- [11] McGrath, T. J., E. T. Selig, and L. C. DiFrancesco, "Stiffness of HDPE Pipe in Ring Bending," in Eckstein, ed., *Buried Plastic Pipe Technology*, Vol. 2, ASTM STP 1222, American Society for Testing and Materials, pp. 195-205, 1994.
- [12] Hogg, P. J., and D. Hull, "Micromechanisms of Crack Growth in Composite Materials under Corrosive Environments," *Metal Science*, pp. 441-449, August-September 1980.
- [13] Pearson, E. L., "Stress Corrosion Performance, Flowrite Sewer Pipe," Owens Corning Internal Data Report, T-91-101-V, May 1997.
- [14] Loos, A. C., G. S. Springer, B. A. Sanders, and R. W. Tung, "Moisture Absorption of Polyester-E Glass Composites," *Journal of Composite Materials*, Vol. 14, pp. 142-154, 1980.

- [15] Phillips, M. G., "Prediction of Long-Term Stress-Rupture Life for Glass Fibre-Reinforced Polyester Composites in Air and Aqueous Environments," *Composites*, pp. 270-275, July 1983.
- [16] Zhurkov, S. N, *International Journal of Fracture Mechanics*, Vol. 1, pp. 311-322, 1965.
- [17] Owens Corning, Excel spreadsheet private communication.
- [18] Agarwal, B. D., and L. J. Broutman, *Analysis and Performance of Fiber Composites*, Second Edition, New York, John Wiley & Sons, Inc., 1990.
- [19] Springer, G. S., "Effects of Temperature and Moisture on Sheet Molding Compounds," *Journal of Reinforced Plastics and Composites*, Vol. 2, pp. 70-89, 1983.
- [20] Pritchard, G., and S. D. Speake, "The Use of Water Absorption Kinetic Data to Predict Laminate Property Changes," *Composites*, pp. 228-232, July 1987.
- [21] Eckstein, D., ed., *Buried Plastic Pipe Technology*, Vol. 2, ASTM STP 1222, American Society for Testing and Materials, 1994.
- [22] Jones, R. M., *Mechanics of Composite Materials*, Hemisphere Publishing Corporation, 1975.
- [23] Reifsnider, K. L., and W. W. Stinchomb, "A Critical Element Model of the Residual Strength and Life of Fatigue Loaded Coupons," in Hahn, ed., *Composite Materials: Fatigue and Fracture*, ASTM STP 907, American Society for Testing and Materials, pp. 298-303, 1986.

- [24] Tsai, S. W., and M. T. Wu, "A General Theory of Strength for Anisotropic Materials," *Journal of Composite Materials*, Vol. 5, pp. 58-80, 1971.

APPENDIX: MATHEMATICA CODE

■ Modules used in the code: diffusion, stress analysis and initial strain.

■ Diffusion module before first ply cracks

```
moisture[Δtime_, delx_, delt_, totinterv_, B_, Dn_] :=  
Module[{cn1, ntime, fac, cinc, Cn, midconc}, {Cn = Dn;  
    fac = delt / delx^2;  
    ntime = Round[Δtime / delt];  
    Do[{Do[{cinc = fac * (B[[i]] * Cn[[i + 1]] -  
        (B[[i - 1]] + B[[i]]) * Cn[[i]] + B[[i - 1]] * Cn[[i - 1]]},  
        cn1[i - 1] = Cn[[i]] + cinc},  
        {i, 2, totinterv}],  
        Do[  
            {Cn[[i]] = cn1[i - 1]}, {i, 2, totinterv}],  
        {t, 1, ntime}],  
    midconc =  
    {Cn[[2]], Cn[[7]], (Cn[[17]] + Cn[[18]]) / 2,  
    Cn[[24]], (Cn[[30]] + Cn[[31]]) / 2, Cn[[38]]};  
{Cn, midconc}]
```

■ Stress Analysis Module (Axi-symmetric solution)

```
stressAxi[con_, temp_, int_, E1_, E2_, E3_, G12_, G13_, G23_, n12_,
  n13_, n23_, alpha_, alpha2_, alpha3_, beta1_, beta2_, beta3_, theta_, th_, r1_, n_] :=
Module[
  {Fx, Tx, beta, S, T, R, epsmoisture, Q, Lambda, K, L, M, r, b, mat, bat, m}, {
```

```
Do[m[i, j] = 0, {i, 1, 2*n+2}, {j, 1, 2*n+2}];
ext := 0;
Fx := 0;
Tx := 0;
```

```
Do[alpha[i] =  $\begin{pmatrix} \alpha1[[i]] \\ \alpha2[[i]] \\ \alpha3[[i]] \\ 0 \\ 0 \\ 0 \end{pmatrix}$ , {i, 1, n}];
```

```
Do[beta[i] =  $\begin{pmatrix} \beta1[[i]] \\ \beta2[[i]] \\ \beta3[[i]] \\ 0 \\ 0 \\ 0 \end{pmatrix}$ , {i, 1, n}];
```

```
Do[S[i] =
```

```
 $\begin{pmatrix} E1[[i]]^{-1} & \frac{-n12[[i]]}{E1[[i]]} & \frac{-n13[[i]]}{E1[[i]]} & 0 & 0 & 0 \\ \frac{-n12[[i]]}{E1[[i]]} & E2[[i]]^{-1} & \frac{-n23[[i]]}{E2[[i]]} & 0 & 0 & 0 \\ \frac{-n13[[i]]}{E1[[i]]} & \frac{-n23[[i]]}{E2[[i]]} & E3[[i]]^{-1} & 0 & 0 & 0 \\ 0 & 0 & 0 & G23[[i]]^{-1} & 0 & 0 \\ 0 & 0 & 0 & 0 & G13[[i]]^{-1} & 0 \\ 0 & 0 & 0 & 0 & 0 & G12[[i]]^{-1} \end{pmatrix},$ 
```

```
{i, 1, n}];
```

```
T[x_] :=
```

```
 $\begin{pmatrix} \cos[x]^2 & \sin[x]^2 & 0 & 0 & 0 & 2 * \cos[x] * \sin[x] \\ \sin[x]^2 & \cos[x]^2 & 0 & 0 & 0 & -2 * \cos[x] * \sin[x] \\ 0 & 0 & 1 & 0 & 0 & 0 \\ 0 & 0 & 0 & \cos[x] & -\sin[x] & 0 \\ 0 & 0 & 0 & \sin[x] & \cos[x] & 0 \\ -\cos[x] * \sin[x] & \cos[x] * \sin[x] & 0 & 0 & 0 & \cos[x]^2 - \sin[x]^2 \end{pmatrix}$ 
```

$$\left. \vphantom{\int} \right\};$$

$$R := \begin{pmatrix} 1 & 0 & 0 & 0 & 0 & 0 \\ 0 & 1 & 0 & 0 & 0 & 0 \\ 0 & 0 & 1 & 0 & 0 & 0 \\ 0 & 0 & 0 & 2 & 0 & 0 \\ 0 & 0 & 0 & 0 & 2 & 0 \\ 0 & 0 & 0 & 0 & 0 & 2 \end{pmatrix};$$

Do[epsmoisture[i] = R . Inverse[T[theta[[i]] * Pi / 180]] . beta[i] * con[[i]] +
R . Inverse[T[theta[[i]] * Pi / 180]] . alpha[i] * temp[[i]], {i, 1, n}];

Do[Q[i] = Inverse[T[theta[[i]] * Pi / 180]] .
Inverse[S[i]] . R . T[theta[[i]] * Pi / 180] . Inverse[R], {i, 1, n}];

Do[Lambda[i] = $\sqrt{\frac{Q[i][[2, 2]]}{Q[i][[3, 3]]}}$, {i, 1, n}];

Do[K[i] = $\frac{Q[i][[1, 2]] - Q[i][[1, 3]]}{Q[i][[3, 3]] - Q[i][[2, 2]]}$, {i, 1, n}];

Do[L[i] = $\frac{Q[i][[2, 6]] - 2 * Q[i][[3, 6]]}{4 * Q[i][[3, 3]] - Q[i][[2, 2]]}$, {i, 1, n}];

Do[M[i] = ((Q[i][[1, 3]] - Q[i][[1, 2]]) * epsmoisture[i][[1]] +
(Q[i][[2, 3]] - Q[i][[2, 2]]) * epsmoisture[i][[2]] +
(Q[i][[3, 3]] - Q[i][[3, 2]]) * epsmoisture[i][[3]] +
(Q[i][[3, 6]] - Q[i][[2, 6]]) * epsmoisture[i][[6]]) /
(Q[i][[3, 3]] - Q[i][[2, 2]]), {i, 1, n}];

Do[r[i] = r1 + $\sum_{j=1}^i$ th[[j]], {i, 1, n}];

Do[b[i] = (-M[i] * (Q[i][[3, 3]] + Q[i][[3, 2]]) +
M[i + 1] * (Q[i + 1][[3, 3]] + Q[i + 1][[3, 2]]) +
(Q[i][[3, 1]] * epsmoisture[i][[1]] +
Q[i][[3, 2]] * epsmoisture[i][[2]] +
Q[i][[3, 3]] * epsmoisture[i][[3]] +
Q[i][[3, 4]] * epsmoisture[i][[4]] +
Q[i][[3, 5]] * epsmoisture[i][[5]] +
Q[i][[3, 6]] * epsmoisture[i][[6]]) -
(Q[i + 1][[3, 1]] * epsmoisture[i + 1][[1]] +
Q[i + 1][[3, 2]] * epsmoisture[i + 1][[2]] +
Q[i + 1][[3, 3]] * epsmoisture[i + 1][[3]] +
Q[i + 1][[3, 4]] * epsmoisture[i + 1][[4]] +
Q[i + 1][[3, 5]] * epsmoisture[i + 1][[5]] +
Q[i + 1][[3, 6]] * epsmoisture[i + 1][[6]]) /
10^9,
{i, 1, n - 1}];

```

Do[b[i + n - 1] = -(M[i] - M[i + 1]) * r[i], {i, 1, n - 1}];
b[2 * n - 1] = (int - M[1] * (Q[1][[3, 3]] + Q[1][[3, 2]]) +
  (Q[1][[3, 1]] * epsmoisture[1][[1]] + Q[1][[3, 2]] *
    epsmoisture[1][[2]] + Q[1][[3, 3]] * epsmoisture[1][[3]] +
    Q[1][[3, 4]] * epsmoisture[1][[4]] +
    Q[1][[3, 5]] * epsmoisture[1][[5]] +
    Q[1][[3, 6]] * epsmoisture[1][[6]])) /
  10^9;
b[2 * n] = (ext - M[n] * (Q[n][[3, 3]] + Q[n][[3, 2]]) +
  (Q[n][[3, 1]] * epsmoisture[n][[1]] + Q[n][[3, 2]] *
    epsmoisture[n][[2]] + Q[n][[3, 3]] * epsmoisture[n][[3]] +
    Q[n][[3, 4]] * epsmoisture[n][[4]] +
    Q[n][[3, 5]] * epsmoisture[n][[5]] +
    Q[n][[3, 6]] * epsmoisture[n][[6]])) /
  10^9;
b[2 * n + 1] =
  Fx - 2 * Pi * ( (r[1]^2 - r1^2) / 2 * ((Q[1][[1, 3]] + Q[1][[1, 2]]) M[1] -
    (Q[1][[1, 1]] * epsmoisture[1][[1]] +
      Q[1][[1, 2]] * epsmoisture[1][[2]] +
      Q[1][[1, 3]] * epsmoisture[1][[3]] +
      Q[1][[1, 4]] * epsmoisture[1][[4]] +
      Q[1][[1, 5]] * epsmoisture[1][[5]] +
      Q[1][[1, 6]] * epsmoisture[1][[6]])) +
    Sum[ ((r[s + 1]^2 - r[s]^2) / 2 *
      ((Q[s + 1][[1, 3]] + Q[s + 1][[1, 2]]) M[s + 1] -
        (Q[s + 1][[1, 1]] * epsmoisture[s + 1][[1]] +
          Q[s + 1][[1, 2]] * epsmoisture[s + 1][[2]] +
          Q[s + 1][[1, 3]] * epsmoisture[s + 1][[3]] +
          Q[s + 1][[1, 4]] * epsmoisture[s + 1][[4]] +
          Q[s + 1][[1, 5]] * epsmoisture[s + 1][[5]] +
          Q[s + 1][[1, 6]] * epsmoisture[s + 1][[6]])))]);
b[2 * n + 2] =
  Tx - 2 * Pi ( (r[1]^3 - r1^3) / 3 * ((Q[1][[6, 3]] + Q[1][[6, 2]]) M[1] -
    (Q[1][[6, 1]] * epsmoisture[1][[1]] +
      Q[1][[6, 2]] * epsmoisture[1][[2]] +
      Q[1][[6, 3]] * epsmoisture[1][[3]] +
      Q[1][[6, 4]] * epsmoisture[1][[4]] +
      Q[1][[6, 5]] * epsmoisture[1][[5]] +
      Q[1][[6, 6]] * epsmoisture[1][[6]])) +
    Sum[ ((r[s + 1]^3 - r[s]^3) / 3 *

```

```

      ((Q[s + 1][[6, 3]] + Q[s + 1][[6, 2]]) M[s + 1] -
      (Q[s + 1][[6, 1]] * epsmoisture[s + 1][[1]] +
      Q[s + 1][[6, 2]] * epsmoisture[s + 1][[2]] +
      Q[s + 1][[6, 3]] * epsmoisture[s + 1][[3]] +
      Q[s + 1][[6, 4]] * epsmoisture[s + 1][[4]] +
      Q[s + 1][[6, 5]] * epsmoisture[s + 1][[5]] +
      Q[s + 1][[6, 6]] * epsmoisture[s + 1][[6]]))
    bat := Table[b[i], {i, 1, 2 * n + 2}];
    Do[{m[i, 2 * i - 1] = (Q[i][[3, 3]] * Lambda[i] * r[i] ^ (Lambda[i] - 1) +
      Q[i][[3, 2]] * r[i] ^ (Lambda[i] - 1)) / 10^9,
      {i, 1, n - 1}}];
    Do[{m[i, 2 * i] = (-Q[i][[3, 3]] * Lambda[i] * r[i] ^ (-Lambda[i] - 1) +
      Q[i][[3, 2]] * r[i] ^ (-Lambda[i] - 1)) / 10^9,
      {i, 1, n - 1}}];
    Do[{m[i, 2 * i + 1] =
      (- (Q[i + 1][[3, 3]] * Lambda[i + 1] * r[i] ^ (Lambda[i + 1] - 1) +
      Q[i + 1][[3, 2]] * r[i] ^ (Lambda[i + 1] - 1))) / 10^9,
      {i, 1, n - 1}}];
    Do[{m[i, 2 * i + 2] =
      (Q[i + 1][[3, 3]] * Lambda[i + 1] * r[i] ^ (-Lambda[i + 1] - 1) -
      Q[i + 1][[3, 2]] * r[i] ^ (-Lambda[i + 1] - 1)) / 10^9,
      {i, 1, n - 1}}];
    Do[{m[i, 2 * n + 1] = ((Q[i][[3, 1]] +
      Q[i][[3, 2]] * K[i] + Q[i][[3, 3]] * K[i]) - (Q[i + 1][[3, 1]] +
      Q[i + 1][[3, 2]] * K[i + 1] + Q[i + 1][[3, 3]] * K[i + 1])) /
      10^9,
      {i, 1, n - 1}}];
    Do[{m[i, 2 * n + 2] =
      (((Q[i][[3, 6]] + Q[i][[3, 2]] * L[i] + 2 * Q[i][[3, 3]] * L[i]) -
      (Q[i + 1][[3, 6]] + Q[i + 1][[3, 2]] * L[i + 1] +
      Q[i + 1][[3, 3]] * 2 * L[i + 1])) *
      r[i]) /
      10^9,
      {i, 1, n - 1}}];
    Do[{m[i + n - 1, 2 * i - 1] = r[i] ^ Lambda[i]}, {i, 1, n - 1}];
    Do[{m[i + n - 1, 2 * i] = r[i] ^ -Lambda[i]}, {i, 1, n - 1}];
    Do[{m[i + n - 1, 2 * i + 1] = -r[i] ^ Lambda[i + 1]}, {i, 1, n - 1}];
    Do[{m[i + n - 1, 2 * i + 2] = -r[i] ^ -Lambda[i + 1]}, {i, 1, n - 1}];
    Do[{m[i + n - 1, 2 * n + 1] = (K[i] - K[i + 1]) r[i]}, {i, 1, n - 1}];
    Do[{m[i + n - 1, 2 * n + 2] = (L[i] - L[i + 1]) r[i] ^ 2}, {i, 1, n - 1}];
    m[2 * n - 1, 1] = (Q[1][[3, 3]] * Lambda[1] * r1 ^ (Lambda[1] - 1) +
      Q[1][[3, 2]] * r1 ^ (Lambda[1] - 1)) / 10^9;
    m[2 * n - 1, 2] = (-Q[1][[3, 3]] * Lambda[1] * r1 ^ (-Lambda[1] - 1) +
      Q[1][[3, 2]] * r1 ^ (-Lambda[1] - 1)) / 10^9;
    m[2 * n - 1, 2 * n + 1] =
      (Q[1][[3, 1]] + (Q[1][[3, 2]] + Q[1][[3, 3]]) * K[1]) / 10^9;

```

```

m[2*n-1, 2*n+2] =
  ((Q[1][[3, 6]] + (Q[1][[3, 2]] + 2*Q[1][[3, 3]]) * L[1]) * r1) / 10^9;
m[2*n, 2*n-1] := (Q[n][[3, 3]] * Lambda[n] * r[n]^(Lambda[n] - 1) +
  Q[n][[3, 2]] * r[n]^(Lambda[n] - 1)) / 10^9;
m[2*n, 2*n] := (-Q[n][[3, 3]] * Lambda[n] * r[n]^(-Lambda[n] - 1) +
  Q[n][[3, 2]] * r[n]^(-Lambda[n] - 1)) / 10^9;
m[2*n, 2*n+1] := (Q[n][[3, 1]] + (Q[n][[3, 2]] + Q[n][[3, 3]]) * K[n]) / 10^9;
m[2*n, 2*n+2] :=
  ((Q[n][[3, 6]] + (Q[n][[3, 2]] + 2*Q[n][[3, 3]]) * L[n]) * r[n]) / 10^9;
m[2*n+1, 1] := 2*Pi (r[1]^(Lambda[1] + 1) - r1^(Lambda[1] + 1)) *
  (Q[1][[1, 3]] * Lambda[1] + Q[1][[2, 1]]) / (Lambda[1] + 1);
m[2*n+1, 2] := 2*Pi (r[1]^(-Lambda[1] + 1) - r1^(-Lambda[1] + 1)) *
  (Q[1][[1, 3]] * Lambda[1] - Q[1][[2, 1]]) / (Lambda[1] - 1);
Do[{m[2*n+1, 2*i+1] =
  2*Pi (r[i+1]^(Lambda[i+1] + 1) - r[i]^(Lambda[i+1] + 1)) *
  (Q[i+1][[1, 3]] * Lambda[i+1] + Q[i+1][[2, 1]]) /
  (Lambda[i+1] + 1)},
  {i, 1, n-1}];
Do[{m[2*n+1, 2*i+2] =
  2*Pi (r[i+1]^(-Lambda[i+1] + 1) - r[i]^(-Lambda[i+1] + 1)) *
  (Q[i+1][[1, 3]] * Lambda[i+1] - Q[i+1][[2, 1]]) /
  (Lambda[i+1] - 1)},
  {i, 1, n-1}];
m[2*n+1, 2*n+1] := 2*Pi  $\left( (r[1]^2 - r1^2) / 2 * \right.$ 
  (Q[1][[1, 3]] * K[1] + Q[1][[1, 2]] * K[1] + Q[1][[1, 1]]) +
   $\sum_{s=1}^{n-1} ((Q[s+1][[1, 3]] + Q[s+1][[1, 2]]) K[s+1] + Q[s+1][[1, 1]]) * \left. \right.$ 
  ((r[s+1]^2 - r[s]^2) / 2));
m[2*n+1, 2*n+2] := 2*Pi  $\left( (r[1]^3 - r1^3) / 3 * \right.$ 
  ((2*Q[1][[1, 3]] + Q[1][[1, 2]]) * L[1] + Q[1][[1, 6]]) +
   $\sum_{s=1}^{n-1} ((Q[s+1][[1, 3]] * 2 + Q[s+1][[1, 2]]) L[s+1] + Q[s+1][[1, 6]]) * \left. \right.$ 
  ((r[s+1]^3 - r[s]^3) / 3));
m[2*n+2, 1] :=
  2*Pi * (Q[1][[2, 6]] + Q[1][[3, 6]] * Lambda[1]) / (Lambda[1] + 2) *
  (r[1]^(Lambda[1] + 2) - r1^(Lambda[1] + 2));
m[2*n+2, 2] :=
  2*Pi * (Q[1][[2, 6]] - Q[1][[3, 6]] * Lambda[1]) / (-Lambda[1] + 2) *
  (r[1]^(-Lambda[1] + 2) - r1^(-Lambda[1] + 2));
Do[m[2*n+2, 2*i+1] = 2*Pi *
  (Q[i+1][[2, 6]] + Q[i+1][[3, 6]] * Lambda[i+1]) / (Lambda[i+1] + 2) *

```



```

      (r[i + 1] ^ (Lambda[i + 1] + 2) - r[i] ^ (Lambda[i + 1] + 2)), {i, 1, n - 1}];
Do[{m[2 * n + 2, 2 * i + 2] = 2 * Pi * (Q[i + 1][[2, 6]] -
      Q[i + 1][[3, 6]] * Lambda[i + 1]) / (-Lambda[i + 1] + 2) *
      (r[i + 1] ^ (-Lambda[i + 1] + 2) - r[i] ^ (-Lambda[i + 1] + 2))},
  {i, 1, n - 1}];
m[2 * n + 2, 2 * n + 1] := 2 * Pi  $\left( (r[1]^3 - r1^3) / 3 * \right.$ 
      ((Q[1][[2, 6]] + Q[1][[3, 6]]) * K[1] + Q[1][[1, 6]]) +
       $\sum_{s=1}^{n-1} ((Q[s + 1][[2, 6]] + Q[s + 1][[3, 6]]) K[s + 1] + Q[s + 1][[1, 6]]) * \left. \right.$ 
      ((r[s + 1]^3 - r[s]^3) / 3));
m[2 * n + 2, 2 * n + 2] := 2 * Pi  $\left( (r[1]^4 - r1^4) / 4 * \right.$ 
      ((Q[1][[2, 6]] + 2 * Q[1][[3, 6]]) * L[1] + Q[1][[6, 6]]) +
       $\sum_{s=1}^{n-1} ((Q[s + 1][[2, 6]] + 2 * Q[s + 1][[3, 6]]) L[s + 1] + Q[s + 1][[6, 6]]) * \left. \right.$ 
      ((r[s + 1]^4 - r[s]^4) / 4));
mat = Table[m[i, j], {i, 1, 2 * n + 2}, {j, 1, 2 * n + 2}];
sol = Inverse[mat] . bat;
mat . sol;
Do[w[i][x_] = sol[[2 * i - 1]] * x ^ (Lambda[i]) + sol[[2 * i]] * x ^ (-Lambda[i]) +
      sol[[2 * n + 1]] K[i] * x + sol[[2 * n + 2]] L[i] * x ^ 2 + M[i] * x, {i, 1, n}];
Do[epsx[i] = sol[[2 * n + 1]] - epsmoisture[i][[1]], {i, 1, n}];
Do[epsth[i][x_] = w[i][x] / x - epsmoisture[i][[2]], {i, 1, n}];
Do[epsr[i][x_] =  $\partial_x$  w[i][x] - epsmoisture[i][[3]], {i, 1, n}];
Do[gammaxth[i][x_] = sol[[2 * n + 2]] * x - epsmoisture[i][[6]], {i, 1, n}];
Do[sigx[i][x_] = Q[i][[1, 1]] * epsx[i] +
      epsth[i][x] * Q[i][[1, 2]] + epsr[i][x] * Q[i][[1, 3]] +
      gammaxth[i][x] * Q[i][[1, 6]] - epsmoisture[i][[5]] * Q[i][[1, 5]] -
      epsmoisture[i][[4]] * Q[i][[1, 4]], {i, 1, n}];
Do[sigth[i][x_] = Q[i][[2, 1]] * epsx[i] +
      epsth[i][x] * Q[i][[2, 2]] + epsr[i][x] * Q[i][[2, 3]] +
      gammaxth[i][x] * Q[i][[2, 6]] - epsmoisture[i][[5]] * Q[i][[2, 5]] -
      epsmoisture[i][[4]] * Q[i][[2, 4]], {i, 1, n}];
Do[sigr[i][x_] = Q[i][[3, 1]] * epsx[i] +
      epsth[i][x] * Q[i][[3, 2]] + epsr[i][x] * Q[i][[3, 3]] +
      gammaxth[i][x] * Q[i][[3, 6]] - epsmoisture[i][[5]] * Q[i][[3, 5]] -
      epsmoisture[i][[4]] * Q[i][[3, 4]], {i, 1, n}];
Do[tau[i][x_] = Q[i][[6, 1]] * epsx[i] +
      epsth[i][x] * Q[i][[6, 2]] + epsr[i][x] * Q[i][[6, 3]] +
      gammaxth[i][x] * Q[i][[6, 6]] - epsmoisture[i][[5]] * Q[i][[6, 5]] -
      epsmoisture[i][[4]] * Q[i][[6, 4]], {i, 1, n}];
sigthavg = {sigth[1][r1 + r[1]] / 2},

```

```

sigth[2] [(r[2] + r[1]) / 2], sigth[3] [(r[2] + r[3]) / 2],
sigth[4] [(r[4] + r[3]) / 2], sigth[5] [(r[5] + r[4]) / 2],
sigth[6] [(r[6] + r[5]) / 2], epsth[6] [r[6]]];};

Return[sigthavg];

```

■ Stress Analysis Module (Bending solution)

■ Module for the conservation of length of the elliptic shape

```

nostr[a_, R_] :=
Module[
{b, c}, { c = Solve[ $\pi (2 * R + a - b) * (1 + (3 * ((a + b) / (2 * R + a - b))^2) /$ 
 $(10 + \sqrt{(4 - 3 * ((a + b) / (2 * R + a - b))^2})) / (2 * \pi * R) == 1,$ 
b] [[1, 1, 2]]];
Return[c];

```

■ Module for the root search

```

mindef[dex_, F_, EI_, R_] :=
Module[{d}, {d =  $\frac{0.148778 (dex + R)^2 * R * F / 2}{EI} - nostr[dex, R]$ };
Return[d];

```

■ Step increment to find root

```

deflx[F_, EI_, R_] :=
Module[{dex}, {
dex1 = 0.13662 * F / 2 * R^3 / EI;
While[
mindef[dex1, F, EI, R] > 10^-7, {
dex1 = dex1 + R / 300}];};
Return[2 * dex1];

```

■ Secant method to find root

```
deflx[F_, EI_, R_] :=  
Module[{dex}, {  
  dex1 = 0.13662 * F / 2 * R^3 / EI;  
  dex2 = 0.5 * R;  
  While[  
    Abs[mindef[dex1, F, EI, R]] > 10^-7, {  
      inw = dex1,  
      dex1 = dex1 -  $\frac{\text{mindef}[\text{dex1}, F, EI, R] (\text{dex1} - \text{dex2})}{\text{mindef}[\text{dex1}, F, EI, R] - \text{mindef}[\text{dex2}, F, EI, R]}$ ,  
      dex2 = inw}];};  
Return[2 * dex1];
```

■ Ring bending module with the nonlinear stress analysis

```

stressbend[Fo_, E11_, E22_, G12_, v12_, θ_, th_, Ra_, width_, n_] :=
Module[{Q, T, R, Qbar, Th, z, Am, Bm, Dm, Ax, Bx, Cx, Dx, Ap, Bp, Dp, Cp, Ma,
Mb, FoA, FoB, Moa, Mob, εA, εB, κA, κB, εAtot, εBtot, σxyAt, σxyAb, σxyBt,
σxyBb, ε12A, σ12At, σ12Ab, ε12B, σ12Bt, σ12Bb, defx, defy}, {
Do[
Q[i] = 
$$\begin{pmatrix} \frac{E11[[i]]}{1-v12[[i]]^2 * \frac{E22[[i]]}{E11[[i]]}} & v12[[i]] * \frac{E22[[i]]}{1-v12[[i]]^2 * \frac{E22[[i]]}{E11[[i]]}} & 0 \\ v12[[i]] * \frac{E22[[i]]}{1-v12[[i]]^2 * \frac{E22[[i]]}{E11[[i]]}} & \frac{E22[[i]]}{1-v12[[i]]^2 * \frac{E22[[i]]}{E11[[i]]}} & 0 \\ 0 & 0 & G12[[i]] \end{pmatrix},$$

{i, 1, n}];
Do[T[i] =

$$\begin{pmatrix} \text{Cos}[\theta[[i]] * \pi / 180]^2 & \text{Sin}[\theta[[i]] * \pi / 180] \\ \text{Sin}[\theta[[i]] * \pi / 180]^2 & \text{Cos}[\theta[[i]] * \pi / 180] \\ -\text{Sin}[\theta[[i]] * \pi / 180] * \text{Cos}[\theta[[i]] * \pi / 180] & \text{Sin}[\theta[[i]] * \pi / 180] * \text{Cos}[\theta[[i]] * \pi / 180] \end{pmatrix},$$

{i, 1, n}];
R := 
$$\begin{pmatrix} 1 & 0 & 0 \\ 0 & 1 & 0 \\ 0 & 0 & 2 \end{pmatrix};$$

Do[Qbar[i] = Dot[Inverse[T[i]], Q[i], R, T[i], Inverse[R]], {i, 1, n}];
Th = Sum[th[[i]], {i, 1, n}];
z = Table[0, {i, 1, n+1}];
Do[{z[[1]] = -Th / 2, z[[i+1]] = z[[i]] + th[[i]]}, {i, 1, n}];
Am = FullSimplify[ $\sum_{i=1}^n$  Qbar[i] * (z[[i+1]] - z[[i]])];
Bm = FullSimplify[ $1/2 * \sum_{i=1}^n$  Qbar[i] * (z[[i+1]]^2 - z[[i]]^2)];
Dm = FullSimplify[ $1/3 * \sum_{i=1}^n$  Qbar[i] * (z[[i+1]]^3 - z[[i]]^3)];
Ax = Inverse[Am];
Bx = -Dot[Inverse[Am], Bm];
Cx = Dot[Bm, Inverse[Am]];
Dx = Dm - Dot[Bm, Inverse[Am], Bm];
Ap = Ax - Dot[Bx, Inverse[Dx], Cx];
Bp = Dot[Bx, Inverse[Dx]];
Cp = Bp;

```

```

Dp = Inverse[Dx];
defx = deflx[Fo, 1 / Dp[[2, 2]] * width, Ra];
Ma = -Fo * (Ra + defx / 2) / π;
Mb = (0.5 - 1 / π) * Fo * (Ra + defx / 2);
defy = 2 * nostr[defx / 2, Ra];

FoA =  $\begin{pmatrix} 0 \\ 0 \\ 0 \end{pmatrix}$ ;

FoB =  $\begin{pmatrix} \text{Fo} / (2 * \text{width}) \\ 0 \\ 0 \end{pmatrix}$ ;

MoA =  $\begin{pmatrix} 0 \\ \text{Ma} / \text{width} \\ 0 \end{pmatrix}$ ;

MoB =  $\begin{pmatrix} 0 \\ \text{Mb} / \text{width} \\ 0 \end{pmatrix}$ ;

εA = Dot[Ap, (FoA)] + Dot[Bp, (MoA)];
κA = Dot[Dp, (MoA)] + Dot[Bp, (FoA)];
εB = Dot[Ap, (FoB)] + Dot[Bp, (MoB)];
κB = Dot[Dp, (MoB)] + Dot[Bp, (FoB)];
εAtot = 100 * (εA + Th / 2 * κA);
εBtot = 100 * (εB + Th / 2 * κB);
Do[{oxytA[i] = Dot[Qbar[i], (εA + κA * z[[i]])]}, {i, 1, n}];
Do[{oxybA[i] = Dot[Qbar[i], (εA + κA * z[[i + 1]])]}, {i, 1, n}];
Do[{oxytB[i] = Dot[Qbar[i], (εB + κB * z[[i]])]}, {i, 1, n}];
Do[{oxybB[i] = Dot[Qbar[i], (εB + κB * z[[i + 1]])]}, {i, 1, n}];
Do[{ε12A[i] = Dot[R, T[i], εA + (z[[i]] + z[[i + 1]]) / 2 * κA], σ12tA[i] =
Dot[T[i], oxytA[i]], σ12bA[i] = Dot[T[i], oxybA[i]]}, {i, 1, n}];
Do[{ε12B[i] = Dot[R, T[i], εB + (z[[i]] + z[[i + 1]]) / 2 * κB],
σ12tB[i] = Dot[T[i], oxytB[i]],
σ12bB[i] = Dot[T[i], oxybB[i]]}, {i, 1, n}];
sigthavg = {σ12tA[1][[1]], σ12tA[2][[1]], σ12tA[3][[1]], σ12tA[4][[1]],
σ12tA[5][[1]], σ12tA[6][[1]], σ12tB[1][[1]], σ12tB[2][[1]],
σ12tB[3][[1]], σ12tB[4][[1]], σ12tB[5][[1]], σ12tB[6][[1]],
εAtot, εBtot, defx, defy, Ma, Mb, Dp[[1, 1]], Dp[[2, 2]]};
};
Return[sigthavg];

```

■ Main Program

■ Diffusivity according to the volume fraction of resin

$$\text{fitdiffu}[f_]= -1.0625 * 10^{-12} * f + 1.32 * 10^{-12};$$

■ Ply properties

■ Ply 1: 90% polyester resin, 10% mat glass

```
cmaxRH[1] = 0.0042;
cmaxW[1] = 0.036;
E1[1][c_, A_] = 3.3 * 10^9 *  $\left(1 - \frac{0.1 * c}{cmaxW[1]}\right) * A$ ;
E2[1][c_, A_] = 3.3 * 10^9 *  $\left(1 - \frac{0.1 * c}{cmaxW[1]}\right) * A$ ;
ν12[1] = ν12[6] = 0.25;
G12[1][c_, A_] = E1[1][c, A] / (2 * (1 + ν12[1])) * A;
Xt[1][c_] = 74.9 * 10^6 *  $\left(1 - \frac{0.35 * c}{cmaxW[1]}\right)$ ;
Yt[1][c_] = 65.9 * 10^6 *  $\left(1 - \frac{0.35 * c}{cmaxW[1]}\right)$ ;
Xc[1][c_] = 167 * 10^6 *  $\left(1 - \frac{0.35 * c}{cmaxW[1]}\right)$ ;
Yc[1][c_] = 146.9 * 10^6 *  $\left(1 - \frac{0.35 * c}{cmaxW[1]}\right)$ ;
diffusivity[1] = fitdiffu[0.1];
α1[1] = 2.585 * 10^-5;
α2[1] = 2.585 * 10^-5;
β1[1] = 0.3;
β2[1] = 0.3;
tr[1][Fa_] = 1019.4-20*Fa;
```

■ Ply 2: 60% polyester resin, 40% chopped glass

```

cmaxRH[2] = 0.0035;
cmaxW[2] = 0.0295;
E1[2][c_, A_] = 5.5 * 10^9 * (1 - (0.2 * c) / cmaxW[2]) * A;
E2[2][c_, A_] = 5.5 * 10^9 * (1 - (0.2 * c) / cmaxW[2]) * A;
ν12[2] = 0.31;
G12[2][c_, A_] = E1[2][c, A] / (2 * (1 + ν12[2])) * A;
Xt[2][c_] = 133.1 * 10^6 * (1 - (0.2 * c) / cmaxW[2]);
Yt[2][c_] = 96.5 * 10^6 * (1 - (0.2 * c) / cmaxW[2]);
Xc[2][c_] = 182.6 * 10^6 * (1 - (0.2 * c) / cmaxW[2]);
Yc[2][c_] = 132.4 * 10^6 * (1 - (0.2 * c) / cmaxW[2]);
diffusivity[2] = fitdiffu[0.4];
α1[2] = 1.585 * 10^-5;
α2[2] = 1.585 * 10^-5;
β1[2] = 0.6;
β2[2] = 0.6;
tr[2][Fa_] = 1019.4 - 20 * Fa;

```

■ Ply 3: 32% polyester resin, 22% chopped glass, 45% hoop wound glass

```

cmaxRH[3] = 0.0095;
cmaxW[3] = 0.035;
E1[3][c_, A_] = 33 * 10^9 * (1 - (0.2 * c / cmaxW[3])) * A;
E2[3][c_, A_] = 12 * 10^9 * (1 - (0.2 * c / cmaxW[3])) * A;
ν12[3] = 0.31;
G12[3][c_, A_] = 3 * 10^9 * (1 - (0.2 * c / cmaxW[3])) * A;
Xt[3][c_] = 590 * 10^6 (1 - (0.11 * c / cmaxW[3]));
Yt[3][c_] = 60 * 10^6 (1 - (0.11 * c / cmaxW[3]));
Xc[3][c_] = 504.8 * 10^6 (1 - (0.11 * c / cmaxW[3]));
Yc[3][c_] = 137 * 10^6 (1 - (0.11 * c / cmaxW[3]));
diffusivity[3] = fitdiffu[0.65];
α1[3] = 5.04 * 10^-6;
α2[3] = α2[5] = 2.585 * 10^-5;
β1[3] = β1[5] = 0.0;
β2[3] = β2[5] = 0.6;
tr[3][Fa_] = 10^(1 - Fa) / 0.0495;

```


■ Ply 4: 27% polyester resin, 8% chopped glass, 2% hoop wound glass, 63% sand

$$\begin{aligned}
 c_{\max W}[4] &= 0.04; \\
 c_{\max RH}[4] &= 0.01; \\
 E1[4][c_, A_] &= 5 * 10^9 * \left(1 - \frac{0.4 * c}{c_{\max W}[4]}\right) * A; \\
 E2[4][c_, A_] &= 4.8 * 10^9 * \left(1 - \frac{0.4 * c}{c_{\max W}[4]}\right) * A; \\
 \nu_{12}[4] &= 0.2; \\
 G12[4][c_, A_] &= E1[4][c, A] / (2 * (1 + \nu_{12}[4])) * A; \\
 X_t[4][c_] &= 58.9 * 10^6 * \left(1 - \frac{0.4 * c}{c_{\max W}[4]}\right); \\
 Y_t[4][c_] &= 22.7 * 10^6 * \left(1 - \frac{0.4 * c}{c_{\max W}[4]}\right); \\
 X_c[4][c_] &= 120 * 10^6 * \left(1 - \frac{0.4 * c}{c_{\max W}[4]}\right); \\
 Y_c[4][c_] &= 45 * 10^6 * \left(1 - \frac{0.4 * c}{c_{\max W}[4]}\right); \\
 \alpha_1[4] &= 2.085 * 10^{-5}; \\
 \alpha_2[4] &= 2.085 * 10^{-5}; \\
 \beta_1[4] &= 0.6; \\
 \beta_2[4] &= 0.8; \\
 tr[4][Fa_] &= 10^{19.4 - 20 * Fa};
 \end{aligned}$$

■ Ply 5: 32% polyester resin, 22% chopped glass, 45% hoop wound glass

```

cmaxRH[5] = 0.0095;
cmaxW[5] = 0.035;
E1[5][c_, A_] = 33 * 10^9 * (1 - (0.2 * c / cmaxW[3])) * A;
E2[5][c_, A_] = 12 * 10^9 * (1 - (0.2 * c / cmaxW[3])) * A;
ν12[5] = 0.31;
G12[5][c_, A_] = 3 * 10^9 * (1 - (0.2 * c / cmaxW[3])) * A;
Xt[5][c_] = 590 * 10^6 (1 - (0.11 * c / cmaxW[3]));
Yt[5][c_] = 60 * 10^6 (1 - (0.11 * c / cmaxW[3]));
Xc[5][c_] = 504.8 * 10^6 (1 - (0.11 * c / cmaxW[3]));
Yc[5][c_] = 137 * 10^6 (1 - (0.11 * c / cmaxW[3]));
diffusivity[5] = fitdiffu[0.65];
α1[5] = 5.04 * 10^-6;
α2[5] = 2.585 * 10^-5;
β1[5] = 0.0;
β2[5] = 0.6;
tr[5][Fa_] = 10^(1 - Fa) / 0.0495;

```

■ Ply 6: 90% polyester resin, 10% mat glass

```

cmaxRH[6] = 0.0042;
cmaxW[6] = 0.036;
E1[6][c_, A_] = 3.3 * 10^9 * (1 - (0.1 * c) / cmaxW[1]) * A;
E2[6][c_, A_] = 3.3 * 10^9 * (1 - (0.1 * c) / cmaxW[1]) * A;
ν12[6] = 0.25;
G12[6][c_, A_] = E1[1][c, A] / (2 * (1 + ν12[1])) * A;
Xt[6][c_] = 74.9 * 10^6 * (1 - (0.35 * c) / cmaxW[1]);
Yt[6][c_] = 65.9 * 10^6 * (1 - (0.35 * c) / cmaxW[1]);
Xc[6][c_] = 167 * 10^6 * (1 - (0.35 * c) / cmaxW[1]);
Yc[6][c_] = 146.9 * 10^6 * (1 - (0.35 * c) / cmaxW[1]);
diffusivity[6] = fitdiffu[0.1];
α1[6] = 2.585 * 10^-5;
α2[6] = 2.585 * 10^-5;
β1[6] = 0.3;
β2[6] = 0.3;
tr[6][Fa_] = 1019.4 - 20 * Fa;

```

■ Diffusion data

```
numbplies = 5;
thick = {0.2*10^-3, 0.8*10^-3, 1.3*10^-3, 1.3*10^-3, 0.2*10^-3};
totthick :=  $\sum_{i=1}^{\text{numbplies}}$  thick[[i]]
diff = {diffusivity[1], diffusivity[2],
        diffusivity[3], diffusivity[5], diffusivity[6]};
minplythick = Min[thick];
delx = minplythick / 2;
maxdiff = Max[diff];
delt = delx^2 / (2.1 * maxdiff);
totinterv = Round[totthick / delx];

delt

delt = 2000;
```

■ Generation of the array of diffusivities, ply interface grid point number, and tables of *cmaxW* and *cmaxRH*

```
lower = 1;
Do[{upper = (lower - 1) + Round[totinterv * thick[[i]] / totthick],
    interface[i] = upper + 1,
    Do[b[j] = diff[[i]], {j, lower, upper}],
    lower = upper + 1},
    {i, 1, numbplies}]
B = Table[b[i], {i, 1, totinterv}];
Interface = Table[interface[i], {i, 1, numbplies}];
CmaxW = Table[cmaxW[i], {i, 1, 6}];
CmaxRH = Table[cmaxRH[i], {i, 1, 6}];
Interface;
```

■ Time control, mechanical load control, and input for stress analysis and moisture initial boundary conditions

```
k = 1.2;
numberOfPlies = numbplies + 1;
width = 1;
dia = 0.6;
theta = {90.0, 90.0, 90.0, 90.0, 90.0, 90.0};
th =
  {0.2*10^-3, 0.8*10^-3, 1.3*10^-3, 4.7*10^-3, 1.3*10^-3, 0.2*10^-3};
r1 = dia / 2;

totalTime = 6000 * 3600;
noSteps = 100;
timeInc = totalTime / noSteps;

inconc = cmaxW[1];
outconc = cmaxRH[6];

cn[1] = inconc;
cn[totinterv + 1] = outconc;
Do[{cn[i] = 0}, {i, 2, totinterv}]
Cn = Table[cn[i], {i, 1, totinterv + 1}];
time = 0;

Do[{time = time + timeInc,
  concent = moisture[timeInc, delx, delt, totinterv, B, Cn],
  T[i, 1] = concent[[2]][[1]],
  T[i, 2] = concent[[2]][[2]],
  T[i, 3] = concent[[2]][[3]],
  T[i, 4] = concent[[2]][[4]],
  T[i, 5] = concent[[2]][[5]],
  T[i, 6] = concent[[2]][[6]],
  Cn = concent[[1]],
  concProfile[i] = concent[[1]]},
  {i, 1, noSteps}]

concen = Table[T[i, j], {i, 1, noSteps}, {j, 1, numberOfPlies}];
```

■ *concen* is the matrix of moisture content with time

```
MatrixForm[concen]
```

■ p_n applied internal pressure and F_o transverse load

```
pn = 29 * 1.013 * 10^5;
Fo = 0;
```

■ Ply properties at a given moisture content corresponding to index i

■ A matrix of damaged ply

```
A = Table[1, {i, 1, noSteps}, {j, 1, numberOfPlies}];
```

■ Generation of the material properties according to environmental effects

```
Do[
  {E11[i] = Table[E1[j][concen[[i, j]], A[[i, j]]], {j, 1, numberOfPlies}},
  E22[i] =
  Table[E2[j][concen[[i, j]], A[[i, j]]], {j, 1, numberOfPlies}},
  g12[i] = g13[i] = g23[i] =
  Table[G12[j][concen[[i, j]], A[[i, j]]], {j, 1, numberOfPlies}}],
{i, 1, noSteps}
alpha1 = Table[α1[i], {i, 1, numberOfPlies}];
alpha2 = alpha3 = Table[α2[i], {i, 1, numberOfPlies}];
beta1 = Table[β1[i], {i, 1, numberOfPlies}];
beta2 = beta3 = Table[β2[i], {i, 1, numberOfPlies}];
n12 = n13 = n23 = Table[ν12[i], {i, 1, numberOfPlies}];
E33 = {3 * 10^9, 3 * 10^9, 3 * 10^9, 3 * 10^9, 3 * 10^9, 3 * 10^9};
temp = {0, 0, 0, 0, 0, 0};

initialstrain = stressbend[Fo, E11[18], E22[18], g12[18], n12, theta, th,
  r1, width, numberOfPlies][[2 * numberOfPlies + 2]][[2, 1]] +
  stressAxi[concen[[1]], temp, -pn, E11[1], E22[1], E33,
  g12[1], g13[1], g23[1], n12, n13, n23, alpha1, alpha2, alpha3,
  beta1,
  beta2, beta3, theta, th, r1, numberOfPlies][[numberOfPlies + 1]][[1]]

deflection = 1 - (2 * r1 - stressbend[Fo, E11[1], E22[1], g12[1], n12, theta,
  th, r1, width, numberOfPlies][[2 * numberOfPlies + 4]]) /
(2 * r1)
```

■ Evaluation of F_a (maximum stress in the hoop direction) in A

```

Do[{{stressaxis[i] = N[Re[stressAxi[concen[[i]], temp, -pn, E11[i], E22[i],
    E33, g12[i], g13[i], g23[i], n12, n13, n23, alpha1, alpha2, alpha3,
    beta1, beta2, beta3, theta, th, r1, numberOfPlies]]],
    stressesbend[i] = N[stressbend[Fo, E11[i],
    E22[i], g12[i], n12, theta, th, r1, width, numberOfPlies]]],
    {i, 1, noSteps},
    {j, 1, numberOfPlies}]

Do[{{
    sigma = stressaxis[i][[j, 1]] + stressesbend[i][[j, 1]],
    If[sigma < 0.0,
        strength = -Xc[j][concen[[i, j]]], strength = Xt[j][concen[[i, j]]],
        Fa[i, j] = sigma / strength,
        tr[i, j] = tr[j][Fa[i, j]],

        sigma = stressaxis[i][[j, 1]] + stressesbend[i][[numberOfPlies + j, 1]],
        If[sigma < 0.0,
            strength = -Xc[j][concen[[i, j]]], strength = Xt[j][concen[[i, j]]],
            Fa[i, numberOfPlies + j] = sigma / strength,
            tr[i, numberOfPlies + j] = tr[j][Fa[i, numberOfPlies + j]]},
    {i, 1, noSteps}, {j, 1, numberOfPlies}]
Faf = Table[Fa[i, j], {i, 1, noSteps}, {j, 1, 2 * numberOfPlies}];
Trupt = Table[tr[i, j], {i, 1, noSteps}, {j, 1, 2 * numberOfPlies}];

```

■ Remaining Strength F_r Evaluation

```

t = Table[{i * timeInc}, {i, 1, noSteps}];
Do[{{If [Fa[1, j] > 1, Fr[1, j] = 0,
    Fr[1, j] = 1 - ((1 - Fa[1, j]) * (t[[1, 1]] / tr[1, j]) ^ k)}},
    {j, 1, 2 * numberOfPlies}];
i = 2;
While[i <= noSteps, {
    Do[{{If[Fa[i, j] > 1, Fr[i, j] = 0,
        {t0 = ((1 - Fr[i - 1, j]) / (1 - Fa[i, j])) ^ (1/k) * tr[i, j],
        Δt = t[[i, 1]] - t[[i - 1, 1]],
        Fr[i, j] = Fr[i - 1, j] -
            (1 - Fa[i, j]) * (((t0 + Δt) / tr[i, j]) ^ k - (t0 / tr[i, j]) ^ k)}},
        {j, 1, 2 * numberOfPlies}]],
    i = i + 1}]
Frf = Table[Fr[i, j], {i, 1, noSteps}, {j, 1, 2 * numberOfPlies}];

```

■ Failure according to *Fa* and *Fr*

```
Do[{
  If[FrF[[i, j]] - Faf[[i, j]] < 0.0, A[[i, j]] = 0.5],
  If[FrF[[i, j + numberOfPlies]] - Faf[[i, j + numberOfPlies]] < 0.0,
    A[[i, j]] = 0.5}],
  {i, 1, noSteps}, {j, 1, numberOfPlies}]

MatrixForm[Faf]

MatrixForm[Trupt]

MatrixForm[FrF]

MatrixForm[A]
```

■ First discount according to matrix A

```
Do[A[[i, 5]] = 0.1, {i, 12, noSteps}]
```

■ Reset the ply properties for new run

```
Do[
  {E11[i] = Table[E1[j][concen[[i, j]], A[[i, j]]], {j, 1, numberOfPlies}},
  E22[i] =
  Table[E2[j][concen[[i, j]], A[[i, j]]], {j, 1, numberOfPlies}},
  g12[i] = g13[i] = g23[i] =
  Table[G12[j][concen[[i, j]], A[[i, j]]], {j, 1, numberOfPlies}},
  {i, 1, noSteps}]
```


VITA

Jean-Matthieu Bodin was born in November of 1974 in the beautiful city of Paris, France. He grew up in Voisins-Le-Bretonneux, a southern suburb of Versailles, France. He attended every school and boarding school in the southern part of Paris due to incompatibility of attitude until he was given his diploma. After two years of mathematics, physics and technology preparation classes at the Lycée Jules Ferry (Versailles), Mr. Bodin was admitted in the Ecole Nationale Supérieure d'Arts et Métiers (Lille and Paris) in 1994. He graduated in 1997 with a B.S. degree in Mechanical Engineering with a major in plastic materials. In August of the same year, he moved to Blacksburg, Virginia, USA, to enroll in the Master's Program of the Department of Engineering Science and Mechanics at Virginia Tech. He joined the Materials Response Group where he conducted his research on mechanics of composites. Upon receiving his Master's degree, Mr. Bodin will do his military service for a period of fifteen months in the French Navy. He plans to return to the United States and continue his work in the field of composite materials in academia or in industries.